

STARS


University of Central Florida
STARS

Electronic Theses and Dissertations, 2004-2019

2005

Interconnection, Interface And Instrumentation For Micromachined Chemical Sensors

Naveenkumar Srinivasaiah Palsandram
University of Central Florida

 Part of the [Electrical and Electronics Commons](#)
Find similar works at: <https://stars.library.ucf.edu/etd>
University of Central Florida Libraries <http://library.ucf.edu>

This Masters Thesis (Open Access) is brought to you for free and open access by STARS. It has been accepted for inclusion in Electronic Theses and Dissertations, 2004-2019 by an authorized administrator of STARS. For more information, please contact STARS@ucf.edu.

STARS Citation

Palsandram, Naveenkumar Srinivasaiah, "Interconnection, Interface And Instrumentation For Micromachined Chemical Sensors" (2005). *Electronic Theses and Dissertations, 2004-2019*. 482.
<https://stars.library.ucf.edu/etd/482>



INTERCONNECTION, INTERFACE AND INSTRUMENTATION FOR
MICROMACHINED CHEMICAL SENSORS

by

NAVEENKUMAR PALSANDRAM
B.E. Karnatak University, 2000

A thesis submitted in partial fulfillment of the requirements
for the degree of Master of Science
in the Department of Electrical and Computer Engineering
in the College of Engineering and Computer Science
at the University of Central Florida
Orlando, Florida

Summer Term
2005

© 2005 Naveenkumar Palsandram

ABSTRACT

In realizing a portable chemical analysis system, adequate partitioning of a reusable component and a disposable is required. For successful implementation of micromachined sensors in an instrument, reliable methods for interconnection and interface are in great demand between these two major parts. This thesis work investigates interconnection methods of micromachined chip devices, a hybrid fluidic interface system, and measurement circuitry for completing instrumentation. The interconnection method based on micromachining and injection molding techniques was developed and an interconnecting microfluidic package was designed, fabricated and tested. Alternatively, a plug-in type design for a large amount of sample flow was designed and demonstrated. For the hybrid interface, sequencing of the chemical analysis was examined and accordingly, syringe containers, a peristaltic pump and pinch valves were assembled to compose a reliable meso-scale fluidic control unit. A potentiostat circuit was modeled using a simulation tool. The simulated output showed its usability toward three-electrode electrochemical microsensors. Using separately fabricated microsensors, the final instrument with two different designs—flow-through and plug-in type was tested for chlorine detection in water samples. The chemical concentration of chlorine ions could be determined from linearly dependent current signals from the instrument.

Dedicated to my parents

ACKNOWLEDGMENTS

I would like to take this opportunity to thank my advisor Dr. Hyoung J. Cho for his support and constant encouragement. His confidence in my abilities has been a great motivation. I would like to thank Dr. Kalpathy Sundaram for his constant support through the course of my Master's program. I am also thankful for their advice in professional career. It has been a pleasure working with them.

I would also like to thank Dr. Thomas X. Wu for agreeing to be my thesis committee in his busy schedule and on short notice. I would like to acknowledge the committee members, Dr. K. B. Sundaram, Dr. Hyoung J. Cho and Dr. Thomas X. Wu who were willing to give encouragement and support this work.

I would like to thank my colleagues in NanoFab and BioMEMS lab and to all my friends whose timely advice and suggestions helped me in achieving my task.

Last but not the least I am greatly indebted to my parents, sisters and their family for their support, encouragement, and love throughout my life, during the stay outside the home and especially in United States.

TABLE OF CONTENTS

LIST OF FIGURES	viii
CHAPTER ONE: INTRODUCTION.....	1
1.1 Literature Review.....	3
1.1.1 Interconnection	3
1.1.2 Hybrid fluidic interface.....	7
1.1.3 Measurement circuitry	11
1.2 Motivation and objective	12
CHAPTER TWO: INTERCONNECTION AND PACKAGING METHOD FOR MICROMACHINED CHEMICAL SENSORS	15
2.1 Interconnecting microfluidic package.....	15
2.2 Plug-in type package.....	19
CHAPTER THREE: HYBRID FLUIDIC INTERFACE	23
3.1 Design and assembly.....	23
CHAPTER FOUR: MEASUREMENT CIRCUITRY	26
4.1 Equivalent circuit for three-electrode cell.....	26
4.2 Design and simulation.....	28
CHAPTER FIVE: RESULTS AND DISCUSSION.....	35
5.1 Interconnection	35
5.1.1 Microfluidic package	35
5.1.2 Plug-in type package.....	36

5.2 Hybrid fluidic system.....	37
5.3 Potentiostat circuit simulation.....	38
5.4 Instrumentation testing.....	42
5.4.1 Micromachined sensor	42
5.4.2 Flow-through sensor instrument	43
5.4.3 Plug-in sensor instrument	45
CHAPTER SIX: CONCLUSION AND FUTURE WORK.....	50
6.1 Conclusion	50
6.2 Future work.....	50
REFERENCES	51

LIST OF FIGURES

Figure 1.1: Fluidic coupler with sleeve around the bore, capillaries inserted into the sleeve coupler[12].	3
Figure 1.2: (a) molded coupler process flow, (b) molded coupler, and (c) post coupler attached to fluidic port[13].	4
Figure 1.3: Fabrication process of o-ring couplers[14].	5
Figure 1.4: Schematic diagram of interconnect (a) flanging operation and (b) assembled structure[15].	5
Figure 1.5: Process flow of integrated polymer sealant interconnector[17].	6
Figure 1.6: Schematic of the micromachinable actuators used in flow control valves[11].	7
Figure 1.7: Schematic cross-sectional view of the complete mechanical assembly of hybrid fluidic system[6].	9
Figure 1.8: Schematic of assembled PDMS membrane onto the fluidic cartridge[6].	10
Figure 1.9: Schematic cross-sectional drawing of the principal components in (a) pump actuator, (b) valve actuator[6].	11
Figure 1.10: Basic potentiostat design.	12
Figure 2.1: Fluidic chambers and fluidic channels, which is on the bottom side of the fluidic package connected to an inlet and outlet of interconnecting tubing on top side through fluidic channels.	16
Figure 2.2: Top, bottom and cross-sectional view with dimensions of a fluidic package.	17
Figure 2.3: Schematic of microfluidic package fabrication by injection molding.	18

Figure 2.4: Cross sectional schematic of interconnecting microfluidic package with multiple sensors for flow through measurement.....	19
Figure 2.5: PRO-E [®] model of the package with design dimensions.	20
Figure 2.6: PRO-E [®] model of the package with sensor based on plug insertion scheme.	21
Figure 2.7: Schematic diagram of stereolithography[41].	22
Figure 3.1: Block diagram of design scheme for a hybrid fluidic system.	23
Figure 3.2: Schematic of hybrid fluidic system.	24
Figure 3.3: Actual view of (a) peristaltic pump and (b) pinch valve.....	25
Figure 4.1: Schematic representation of potential gradients in a three-electrode cell: (a) $i=0$; (b) $i \neq 0$. Redrawn from [38].....	26
Figure 4.2: Equivalent circuit of a three electrode cell.....	28
Figure 4.3: Block diagram of the measuring system for three electrode amperometric chemical sensor.	29
Figure 4.4: Schematic diagram of the potentiostat circuit.	30
Figure 4.5: Circuit for current-voltage conversion.	31
Figure 4.6: Circuit diagram of potentiostat for amperometric measurements in three electrode chemical sensor.	33
Figure 5.1: SEM picture of the interconnection hole in fluidic channel.....	35
Figure 5.2: Interconnected fluidic packages.	35
Figure 5.3: Assembled view of the microfluidic package with a chip based sensor.	36
Figure 5.4: Assembled view of the plug-in type package with micromachined sensor. ..	36
Figure 5.5: Hybrid fluidic system.	37

Figure 5.6: Flow rate as a function of resistance.	38
Figure 5.7: Block diagram of the potentiostatic circuit including equivalent circuit of an electrochemical cell.	39
Figure 5.8: Time variation for current output at the working electrode.	40
Figure 5.9: Current output for varying bulk resistance values corresponding to KCl concentration.	40
Figure 5.10: Voltage output for varying bulk resistance values corresponding to KCl concentration.	41
Figure 5.11: Dimensions of the three terminal amperometric chlorine sensor (a) flow-through type sensor, (b) plug-in type sensor.	42
Figure 5.12: Fabricated sensors (a) flow-through type sensor, (b) plug-in type sensor. ..	43
Figure 5.13: Experimental setup for flow through measurement.	44
Figure 5.14: Time variation of sensor output measured in a solution with 1.6ppm chlorine under flow through conditions.	44
Figure 5.15: Sensor output current as a function of chlorine concentration.	45
Figure 5.16: Cyclic polarization curve obtained from microfluidic packaged chlorine sensor using 0.1M KCl solution.	46
Figure 5.17: Time variation of sensor output measured in 0.1M KCl solution at static condition for chlorine concentration.	47
Figure 5.18: Sensor output current as a function of KCl concentration.	47
Figure 5.19: Experimental setup for dynamic condition measurement using plug-in type packaged chlorine sensor.	48

Figure 5.20: Time variation of sensor output measured in 0.4M KCl solution at dynamic condition for chlorine concentration..... 49

CHAPTER ONE: INTRODUCTION

"No matter how vast your knowledge or how modest, it is your own mind that has to acquire it. It is only with your own knowledge that you can deal. It is only your own knowledge that you can claim to possess or ask others to consider. Your mind is your only judge of truth — and if others dissent from your verdict, reality is the court of final appeal. Nothing but a man's mind can perform that complex, delicate, crucial process of identification which is thinking. Nothing can direct the process but his own judgment. Nothing can direct his judgment but his moral integrity."

Ayn Rand, 1978

There has been a rapid progress in the development of micrototal analysis systems (μ TAS), where complete chemical analysis or sensing can be performed in a compact instrument [1, 2]. The precisely defined sample volumes as well as the automated control over the microflows offer the potential for greatly improved speed and sensitivity of the instrument compared with the conventional glassware-based apparatus [3]. The progress in the field was originally enabled from developments in analytical chemistry and traditional precision engineering. However, after the introduction of innovative micromachining techniques, which combine traditional 3-D manufacturing methods such as electroplating, and molding with non-traditional 2-D semiconductor fabrication process such as thin film deposition and lithography, major breakthroughs have taken place as can be seen in DNA microarray [4]. Unlike the pure electrical components and

instrument, in realizing this type of instruments, generic challenges include the partitioning of the various components in an instrument. The power supply, heaters, the mechanism for getting the sample into and out of the instrument, providing fresh viable reagents, and the detection method and sensors must be carefully considered [4, 5]. Depending on the application, the electronics, and the power for the fluidic handling mechanism may be interfaced with the disposable microfluidic and/or sensing component. For the chemical analysis instrumentation, the partitioning design, in which the whole instrument is divided into a hybrid fluidic system and a disposable chip, has been a viable approach. The viability of a compact hybrid fluidic system relies on the sophisticated and robust miniature fluidic components as well as control and measurement circuitry that can be easily interfaced with the micromachined disposable chemical sensor [6]. Although a variety of microfluidic components have been developed to control the movement of fluids, (for example, using acoustic, centrifugal, electromagnetic and pneumatic forces) [7-11], the components must be selected carefully to form a compact instrument. In addition, the interface/interconnection between the system and the disposable is of critical importance for the successful instrumentation.

In this work, the subjects of interconnection as a part of disposable chip, a hybrid fluidic system as an interface to a disposable chip and measurement circuitry for instrumentation are investigated to realize a compact and portable chemical analysis system.

1.1 Literature Review

1.1.1 Interconnection

MEMS fluidic devices have long been plagued by the lack of an efficient and convenient means of connection to the outside world or even to other MEMS devices. According to A. Puntambekar “one of the non-trivial challenges in the successful incorporation of a microfluidic component in the system has been the development of reliable microfluidic interconnection technologies which connect the micro-scale devices to the macro-world”. Until now, many micromachined fluidic devices incorporate connections formed by manually gluing tubes to input/output ports.

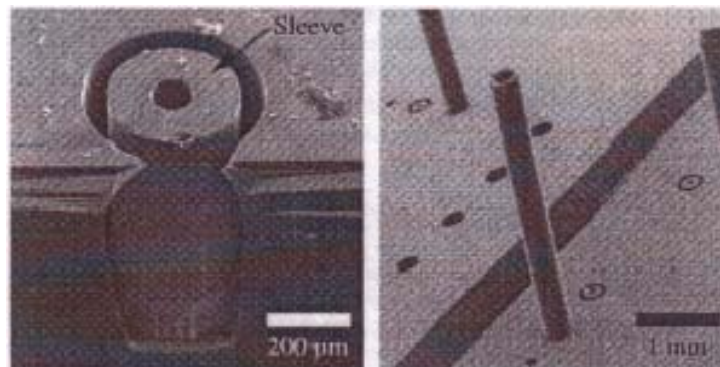


Figure 1.1: Fluidic coupler with sleeve around the bore, capillaries inserted into the sleeve coupler[12].

Figure 1.1 shows an interconnection technique in which coupler is created on silicon substrate with deep reactive ion etching (DRIE) [12]. In this technique holes are drilled using DRIE and matched with the inside outside diameter of the capillaries. The capillary is inserted into the coupler opening and held with adhesive. This technique uses a DRIE process, which is very expensive and thus not suitable for a disposable component. This approach uses silicon sleeve as coupler material which is brittle in

nature and needs an extra step of adhesive bonding to hold the capillary/silicon interface. The sleeve enhances the mechanical integrity of the coupling, but there is a chance of introducing an additional dead volume during the process.

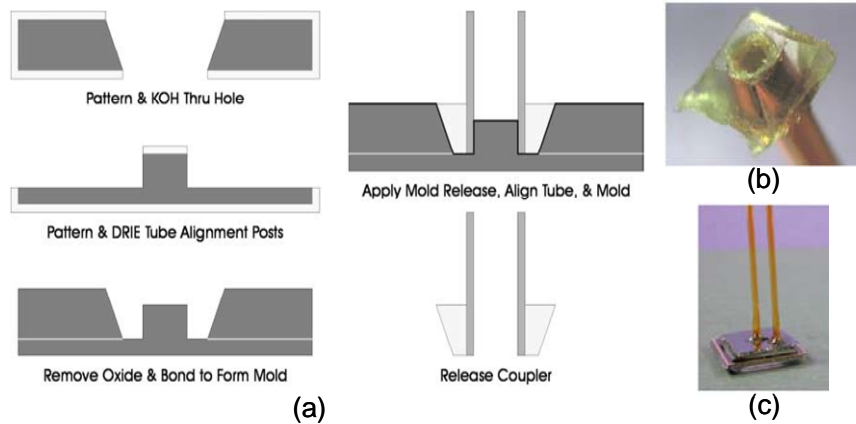


Figure 1.2: (a) molded coupler process flow, (b) molded coupler, and (c) post coupler attached to fluidic port[13].

Figure 1.2 shows another way of interconnecting tubing to fluidic port by introducing intermediate coupler that accurately mates the tubing and port. The mold is fabricated from two bonded silicon wafers (fig 1.2a). One is an oxidized wafer etched with KOH to create through-holes; the other wafer is dry etched to form a circular peg. The peg forms alignment structure for tubing. By bonding these two structures together and coating them with a PTFE release layer, a mold is formed [13]. Moldings are realized by melting raw material such as polyolefin around fused silica tubing fitted on mold posts and releasing when cool (fig 1.2b). Released structures are then attached to fluidic ports simply by re-heating polyolefin, allowing it to reflow and adhere to silicon port (fig 1.2c). This technique needs an extra step for fabricating mold using DRIE process which is of high cost, and it also needs post processing of thermal bonding.

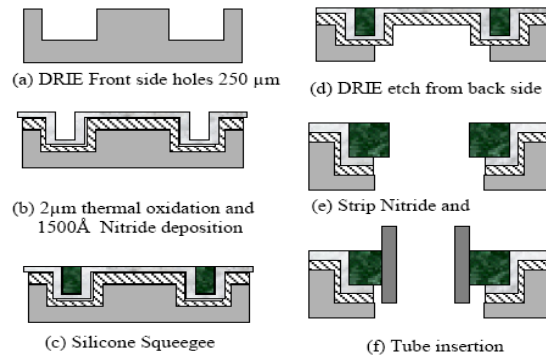


Figure 1.3: Fabrication process of o-ring couplers[14].

Figure 1.3 shows another way of interconnecting tubing to port by o-ring rubber coupler. The process of fabricating coupler starts with etching silicon substrate by DRIE to define o-ring shape (fig 1.3a). Then silicon-di-oxide layer is thermally grown followed by silicon-nitride deposition to serve as adhesion layer between substrate and silicone rubber (fig 1.3b). The silicone rubber is squeezed into the DRIE cavities to form the o-ring (fig 1.3c). Then DRIE etching is done on backside of the substrate to form backside hole (fig 1.3d). The oxide and nitride membranes are then stripped, using chemical etchants (fig 1.3e). The tube is inserted in the hole, and the rubber o-ring deforms to establish a good seal (fig 1.3f) [14]. The process is long and complicated, which is not adequate for producing an inexpensive component. Furthermore, the application of this approach is limited to silicon substrate.

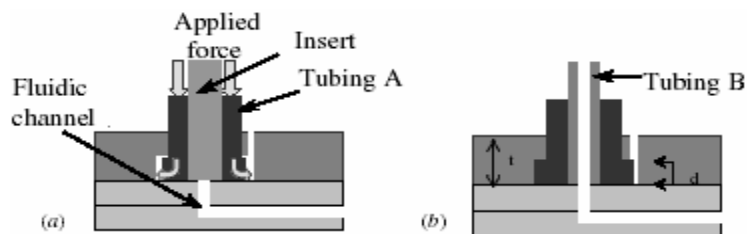


Figure 1.4: Schematic diagram of interconnect (a) flanging operation and (b) assembled structure[15].

Figure 1.4 shows another interconnecting method used for glass- and plastic-based microfluidic systems. In this technique, holes are drilled on glass or polymer substrate and polymer tubings are inserted. Interconnections are formed by deformation on polymer tubings which serves as flanges [15]. Since the holes are formed separately, alignment with the microfluidic channels could be difficult. Thermal bonding is needed as post-process. Although Pattekar and Kothare have proposed a modified approach for the previous technique compatible for high temperature and pressure, the same technical challenge remains [16]. In their approach, they use formation of flange on Teflon tubing by thermal deformation. High temperature epoxy bonding is used for reinforcement of the interconnection.

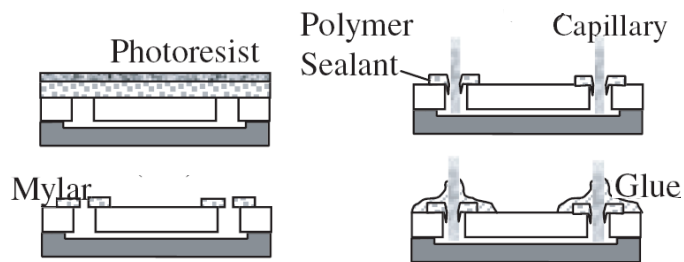


Figure 1.5: Process flow of integrated polymer sealant interconnector[17].

Figure 1.5 shows another technique of fluidic interconnector using an integrated polymer sealant. First, holes are drilled on a Pyrex glass wafer, a Mylar (DuPont Mylar 50M44) film is attached to glass wafer by a thermal bonding process. After the Mylar film is bonded onto the wafer, a photoresist is spun on and patterned as an etchant mask. The Mylar film is patterned by oxygen plasma. The remaining Mylar film is used as the integrated polymer sealant to assist the micro-to-macro interconnection. A capillary tube

is then inserted through the polymer sealant, then a droplet of room-temperature curing (instant glue) is applied to enhance the bonding strength [17]. The extra step for adhesive bonding is still needed in this method.

1.1.2 Hybrid fluidic interface

An intermediate scale of the system is required for driving fluids to a reactor or sensor surface. For driving and routing microflows, various types of micro-pumps [18-20] and microvalves [21, 22] have been studied. For some applications the reduction in size itself is critical (e.g. minimal invasive surgery). For other applications however, it is the precise control of small amounts of fluids (e.g. chemical analysis system), the reduced consumption of reagents (e.g. screening) or the capability of building integrated systems with reduced power consumption (e.g. portable health monitoring) [11] that is critical. This thesis focuses more on the adequate selection and interface of the discrete pumps and valves than on the development of individual components. A mesoscale hybrid fluidic system has been studied as an interface to a chip device [6].

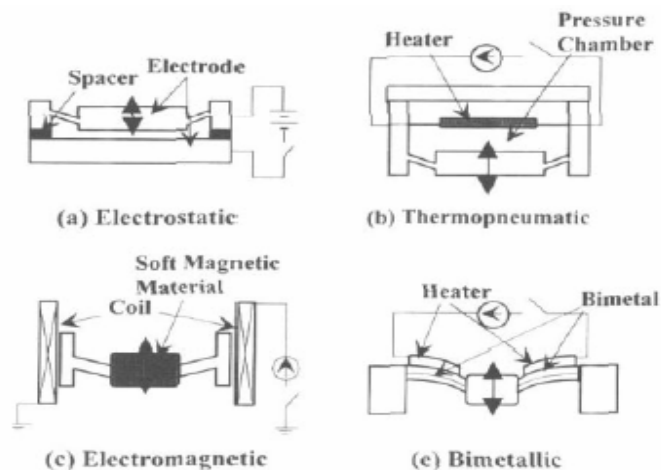


Figure 1.6: Schematic of the micromachinable actuators used in flow control valves[11].

Microvalves: during the last few years a wide variety of microvalves has been developed by many research groups [23, 24]. Different types of valves have been developed using various driving principles shown in Fig 1.6 such as electrostatic, thermopneumatic, electromagnetic and bimetallic actuation. Among those, commercially available microvalves include a bimetallic-driven microvalve manufactured by IC-Sensors [25], a thermopneumatic valve manufactured by Redwood Microsystems [26] and a pneumatically-actuated elastomer (PDMS) membrane valves manufactured by Hoerbiger-Origa-Pneumatics [27]. While dealing with chemical samples in analytical chemistry, often the pinch valve is preferred due to non-contact operation of the valve with the chemical samples. Since the valve shuts off the flow by pinching the tubing not by interacting with the sample itself, any possible chemical interference or contamination can be prevented [28]. A low power, small scale pinch valves are commercially available from Bio-Chem Valve Inc.

Micropumps: The pump mechanisms are based either on traditional hydraulic pump or electro hydrodynamic, electroosmotic, or traveling wave principles [29]. For commercial products, a micromachined flat-walled valveless diffuser pumps (Techno valves, Sweden) [6, 30] and VAMP (valve and micropump) have been developed (Microvalves, Germany). The VAMP device could be used either as an active microvalve or as a forward and reverse working micropump [31]. An extensive review can be found in the Woias's article [32]. A commercially available miniaturized peristaltic pump (Instech Laboratories, Inc) can offer a wide range of pumping rates and self-priming function without contacting the chemical samples.

Hybrid fluidic system: Figure 1.7 shows the hybrid macro-micro fluidics system for a chip-based sensor developed by C.R. Tamanaha et al[6]. The fluidics system consists of four discrete components: (1) a flow cell mounted on top of the sensor chip; (2) a PDMS membrane into which pump and valve membranes and fluid reservoirs have been molded; (3) the plastic fluidics cartridge, which houses the sensor chip and fluidics; and (4) the pump and valve actuator system.

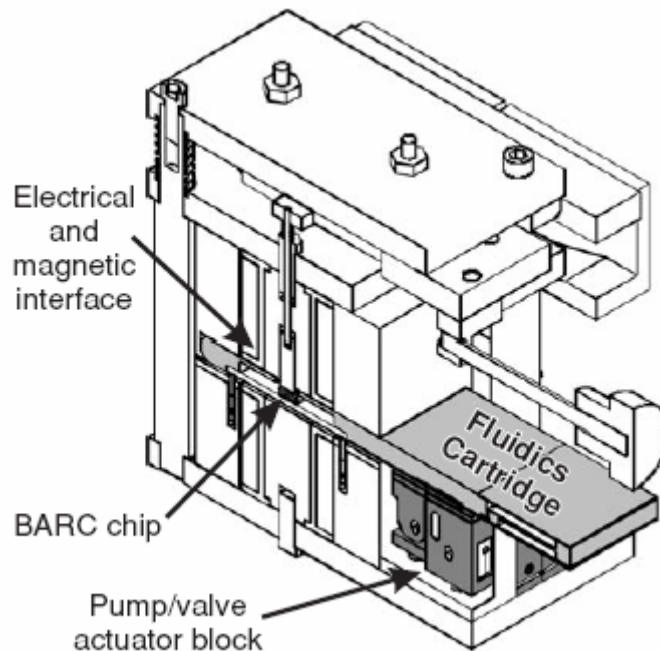


Figure 1.7: Schematic cross-sectional view of the complete mechanical assembly of hybrid fluidic system[6].

The pump and pinch valves are molded using positive relief brass mold on PDMS membrane. The active component of the membrane is the dual-chamber PDMS pump, based on the valveless diffuser/nozzle pump principle. Figure 1.8 shows the assembled PDMS membrane with fluidic cartridge. The microfluidics is driven by the pump and valve actuators contained in the external unit that interfaces kinematically with the PDMS

membrane on the cartridge. Figure 1.9a shows the schematic of principal components in a pump actuator. The actuator is a simple-lever, flexure-hinge displacement amplifier that increases the motion of a piezoelectric stack. The horizontal motion of piezoelectric stack is transferred by the lever and strap linkage into an amplified vertical motion of the pump interface plunger. Figure 1.9b shows the schematic of principal components in a valve actuator. The actuator is a cantilever operated by shape memory alloy (SMA) wire. The open/close of microfluidic channel is performed by locally compressing the pliable PDMS membrane channels. When current is applied, the SMA wire shrinks in length, causing the cantilever to bend downwards. The biasing spring allows the cantilever to return to its starting position once the power to the wire is removed.

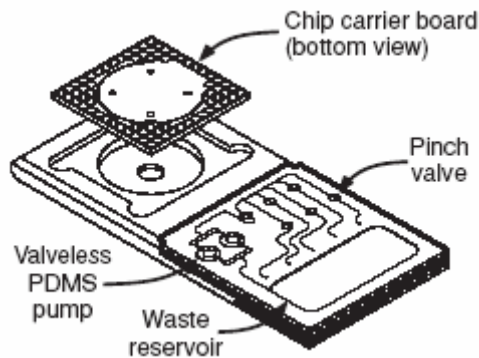


Figure 1.8: Schematic of assembled PDMS membrane onto the fluidic cartridge[6].

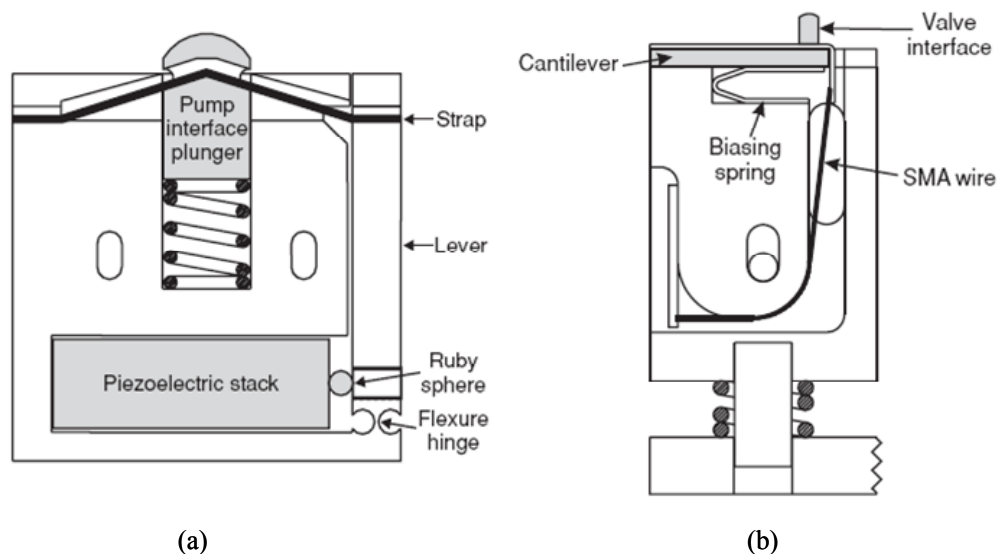


Figure 1.9: Schematic cross-sectional drawing of the principal components in (a) pump actuator, (b) valve actuator[6].

1.1.3 Measurement circuitry

Chemical sensing is a part of information acquisition process in which some insight is obtained about the chemical composition of the system in real time. The group of electrochemical sensors is the widest and oldest of chemical sensors. Some have achieved commercialization but others are still under development[33]. Among those, amperometric sensors use transference of ionic to electronic charges between electroactive species and electrode. When the species is oxidized or reduced at an electrode, the current produced is directly related to concentration of the species. All the electrochemical variables are analog, so suitable circuitry for controlling and measuring voltages, currents and charges in analog domain is needed. The circuit elements best suited to these jobs are operational amplifiers[34]. Since 1942 when Hickling built the first three electrode potentiostat using operational amplifiers, a lot of research has been done to build better potentiostat [35-37].

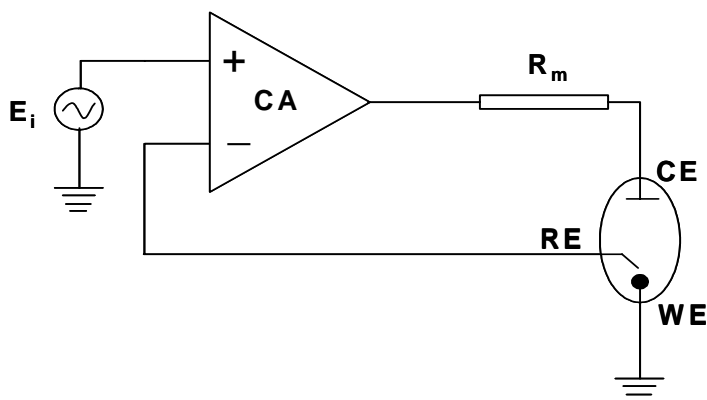


Figure 1.10: Basic potentiostat design.

The potentiostat circuit measures the potential difference between the working and reference electrode, applies the current through the counter electrode and measures the current as an iR drop over the series resistor R_m (fig 1.10). The control amplifier CA is responsible for keeping the voltage between the reference and the working electrode as close as possible to the voltage of the input source E_i . It adjusts its output automatically to control the cell current [34, 38]. Various instrumentation designs have been developed by the researchers using OpAmp to fulfill a simple, reliable and portable amperometric measuring system [39].

1.2 Motivation and objective

In the development of a compact and portable instrument for chemical analysis, as discussed in the introduction, adequate partition of the instrument—a disposable chip, interconnection, a hybrid fluidic system and measurement circuitry—is required. For handling liquid samples in such instrument, an efficient method for interface/interconnection between a disposable chip (microelectrodes) and a hybrid

fluidic system (with macro pumps and valves) is in great demand. The interconnection as a part of microfluidic packaging is challenging because of a lack of a standard platform. For this purpose, as shown in the review, holes are usually drilled on glass or polymer and substrate, which are later used for the insertion of tubes[15, 16]. In this approach, interconnection is often completed by adhesive or thermal bonding. However, there are many drawbacks involved in this process: defect formation during hole formation, misalignment of holes and time-consuming post-processing of the tubing attachment. Adopting an idea from the existing model of IC packages, in which pins and connection pads with standardized pitch and grid dimensions are used for the interconnections, this work intends to develop a reliable, interconnecting method. This can serve as a standardized platform and provide easy connectivity between different microfluidic devices and to a hybrid fluidic system. This work further investigated two-piece plug-in type package as an alternative platform, with interlocking lip for alignment clasps to hold the micromachined sensor for easy connectivity.

In addition to “standardized model,” another issue in the microfluidic devices and systems is “partitioning,” whereby disposable (replaceable) and reusable components are separately fabricated and interfaced to complete an instrument[4]. A hybrid fluidic interface system is needed in this type of approach as reusable component[6]. This work also focuses on designing separate reusable hybrid fluidic interface system from commercially available products.

Finally, the design of measurement circuitry based on amperometric sensing, which will communicate signals with micromachined electrodes, is the subject of the study for completing the instrument.

CHAPTER TWO: INTERCONNECTION AND PACKAGING METHOD FOR MICROMACHINED CHEMICAL SENSORS

A one piece microfluidic package was designed to assemble with micromachined chemical sensor. The microfluidic package was assembled on top of the micromachined sensor chip to enable flow through sample measurement sensor scheme. The microfluidic package inlet/outlet ports were designed so that they can be interconnected to use multiple sensors for a single sample flow. The sample would be introduced into the package by hybrid fluidic interface driven by peristaltic pump and pinch valves for flow through measurement. Alternatively a two—piece plug-in type of package was designed to hold micromachined sensor and contact leads; the package inserts itself in a tubing of sample flow stream for water quality monitoring without sample extraction. The plug-in type package was fabricated using liquid photopolymer resin by micro stereolithography (Micro-STL)[40]. PalmSens potentiostat (Palm Instruments BV.) was used to take the measurements.

2.1 Interconnecting microfluidic package

The microfluidic package was designed to accommodate micromachined chip based sensor. The fluidic package has an inlet and an outlet on one side to standard tubing connection while accommodating the fluidic channels and fluidic chamber on the other side. The schematic view of fluidic package structure with interconnecting tubing dimensions is shown in figure 2.1.

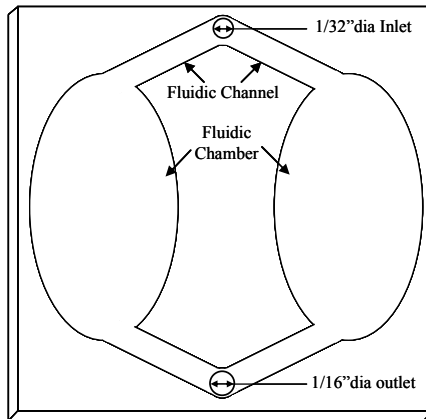


Figure 2.1: Fluidic chambers and fluidic channels, which is on the bottom side of the fluidic package connected to an inlet and outlet of interconnecting tubing on top side through fluidic channels.

The chamber houses the sample solution and the sensor electrode. The analyte enters the chamber through the fluidic channels which connect the chamber to an inlet and outlet. The design of fluidic package was done using the CAD tool. Figure 2.2 shows the dimensions of the designed fluidic package. Aligning holes were included for precise assembling of the package with the sensor chip.

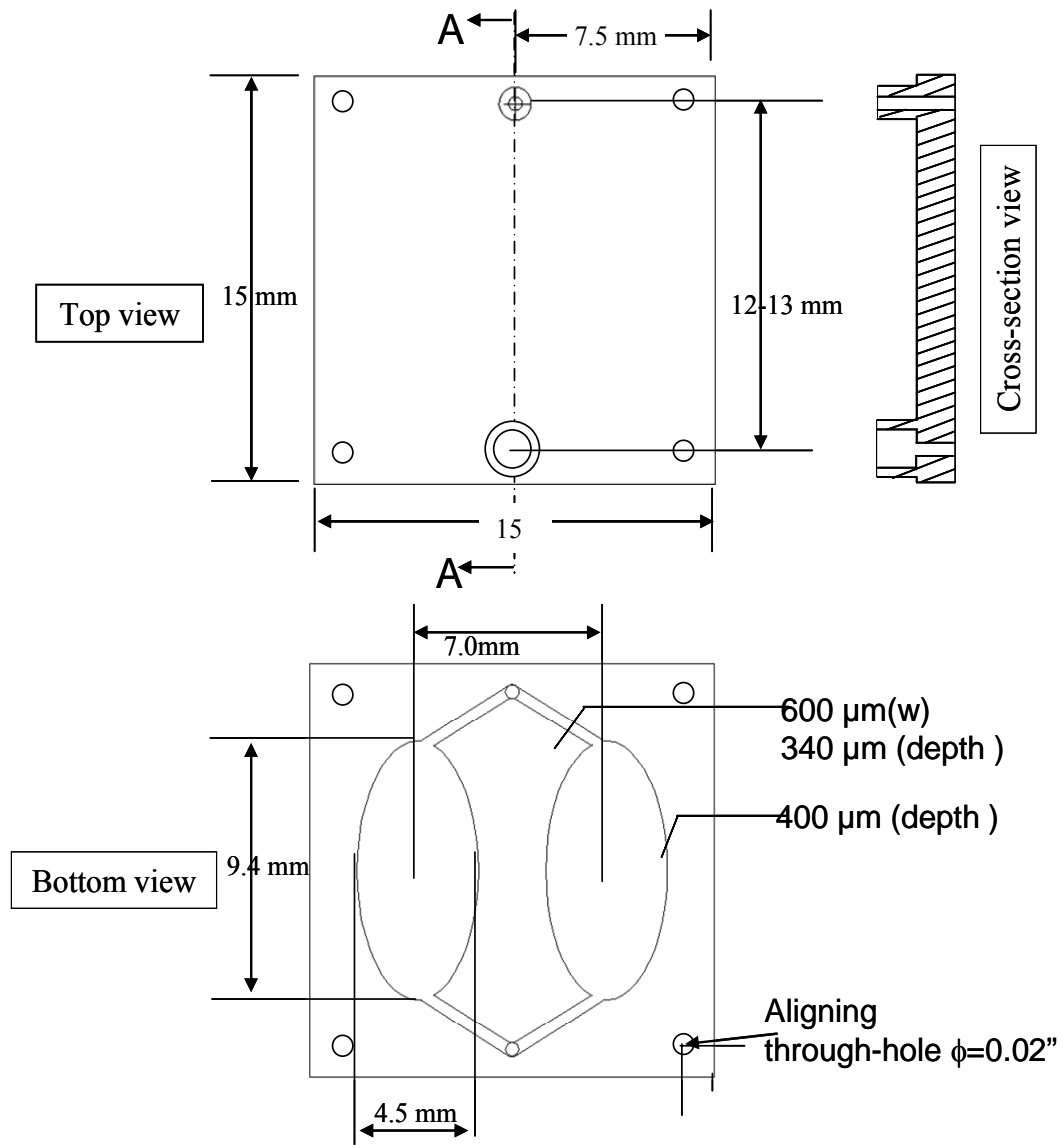


Figure 2.2: Top, bottom and cross-sectional view with dimensions of a fluidic package.

The microfluidic package was fabricated by injection molding using COC (cyclic olefin copolymer) resin. Figure 2.3 shows the schematic of the injection molding fabrication method for microfluidic package.

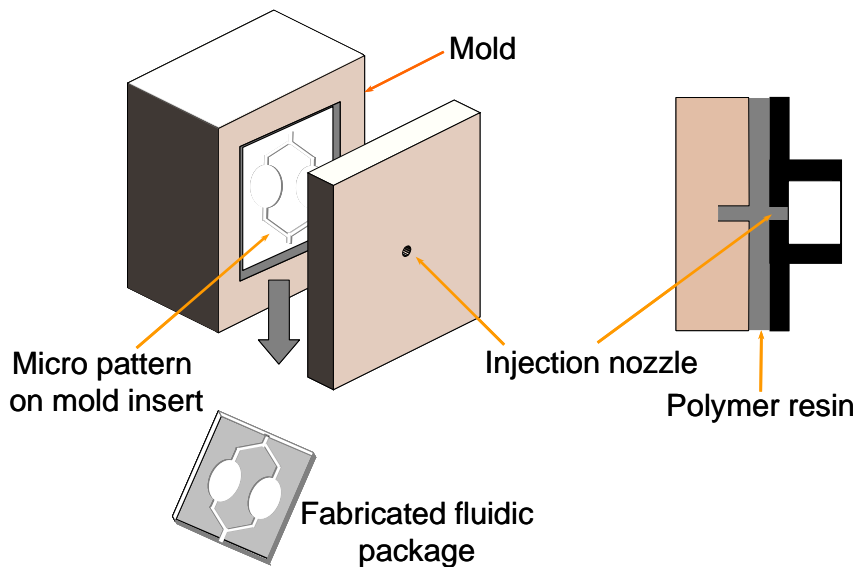


Figure 2.3: Schematic of microfluidic package fabrication by injection molding.

The COC polymer resin is heated to form liquid and injected into the mold, after injection the mold is cooled and fabricated microfluidic package is taken out of the mold. The interconnecting tubes, holes and channels were completed with predefined mold. Therefore, any extra step of bonding or alignment was not necessary. The complicated packaging issue was solved with one body construction of “standardized” tubing connections (1/32”dia inlet and 1/16”dia outlet), which gives great benefit to microfluidic devices.

The inlet/outlet interconnecting tubing were designed in such a way that they can be snapped in together. The internal diameter of the outlet is same as the outer diameter of the inlet. This design enables connecting multiple devices for a single sample flow using the standardized package platform.

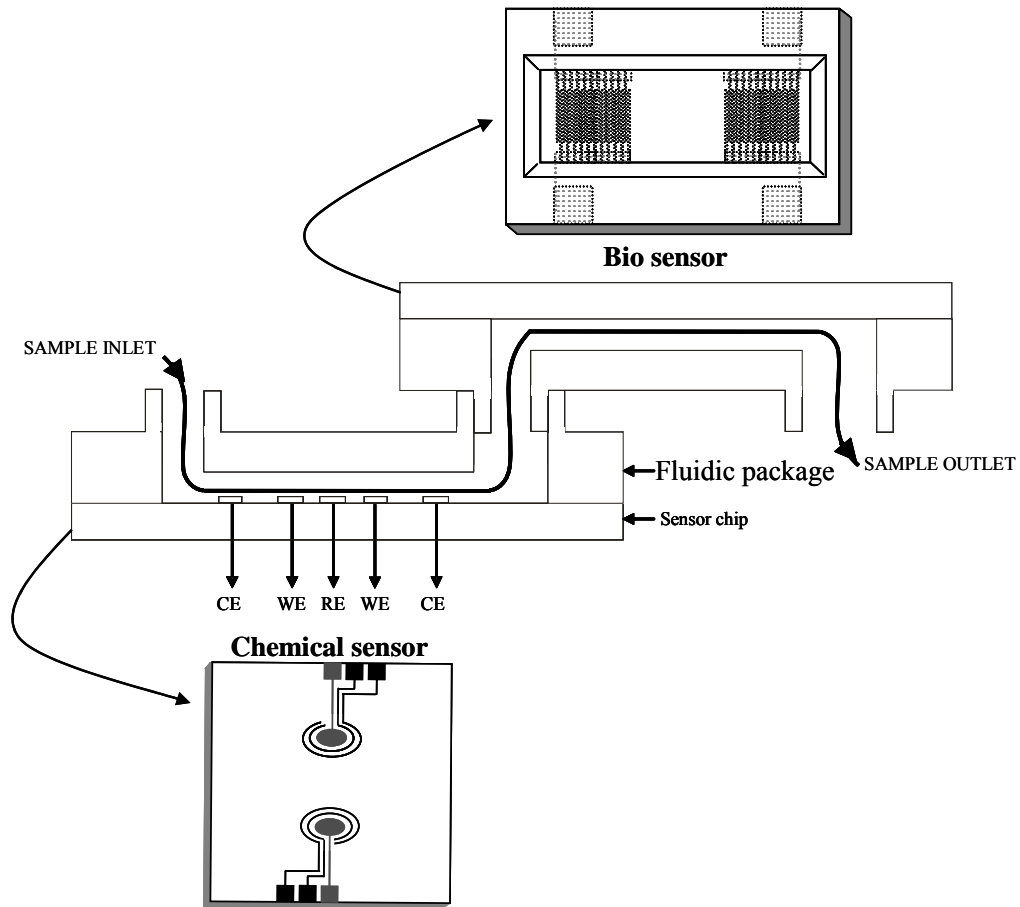


Figure 2.4: Cross sectional schematic of interconnecting microfluidic package with multiple sensors for flow through measurement.

Figure 2.4 presents the idea of interconnecting multiple microfluidic packages for different sensors. Depending on the requirement of the sensor device, the channel side of the package can accommodate different structures while maintaining the same interconnections on the other side of the package.

2.2 Plug-in type package.

The plug-in type package was designed as an alternative way of an interconnection between the micromachined sensor and the sample flow. The package is

made of two pieces which snaps in together holding the sensor in between. The package was designed to connect either right or left hand side contact pads of the sensor. Figure 2.5 shows the designed 3-D model of the package with dimensions. The outer diameter of the whole package was designed to fit the standard tubing size of 3/8". The sensor would be inserted into standard T-connectors for dip-in flow-through measurement. This method of interface is suitable for a flow of samples in large quantity while using microelectrodes for sensing component

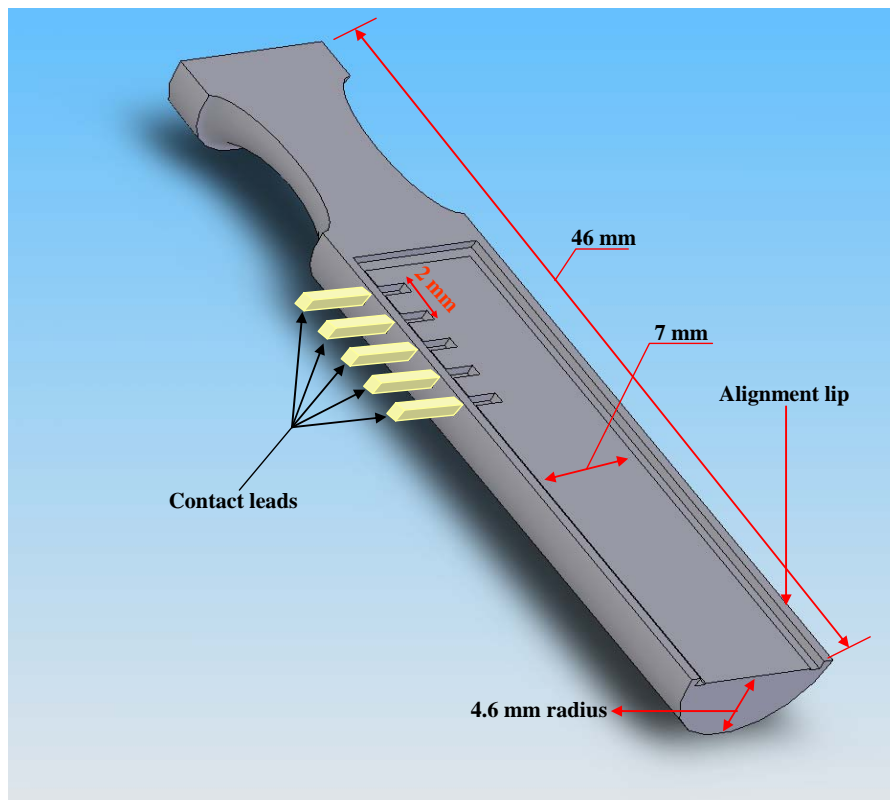


Figure 2.5: PRO-E[®] model of the package with design dimensions.

The package was designed to have an interlocking lip for alignment and clasps to hold the micromachined sensor. The plug-in type package was fabricated using liquid

photopolymer resin by micro stereolithography. Figure 2.6 shows the PRO-E[®] model of the designed package with sensor for plug insertion scheme.

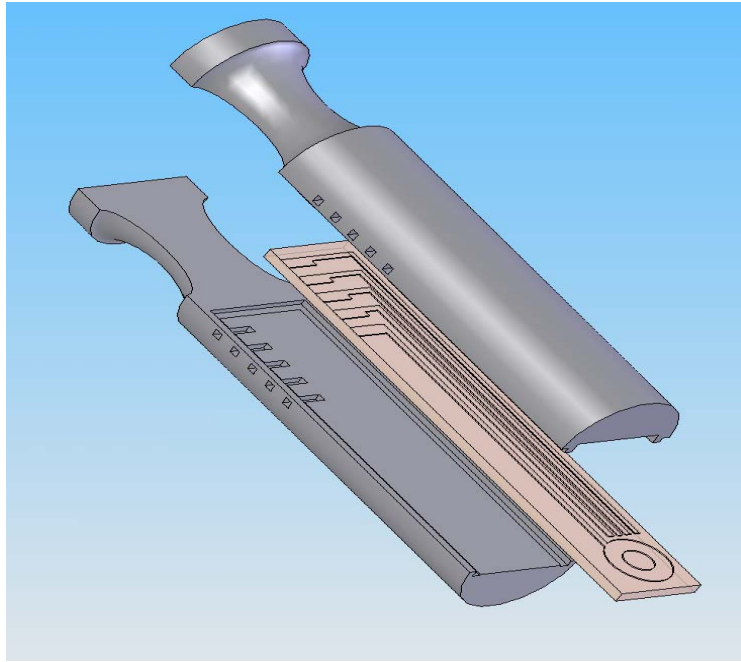


Figure 2.6: PRO-E[®] model of the package with sensor based on plug insertion scheme.

In micro stereolithography, a liquid photopolymer resin is selectively cured using an ultraviolet beam of laser. Figure 2.7 shows the schematic diagram of stereolithography. The machine's software slices the CAD model of the 3D shape of the package to be produced into the required layers. The computer directs the laser beam by means of a set of galvanometer-controlled mirrors. A horizontal elevator tray supports the layer of cured resin. As soon as a layer is finished, the elevator tray lowers one step to submerge the finished layer and fresh (liquid) resin floods onto the surface, covering it ready for the next layer. Each layer neatly bonds to the previous layer. In this way,

building layer by layer the complete model is finished. After the final layer is finished, it can be removed from the tray for final curing and cleaning up of residual resin.

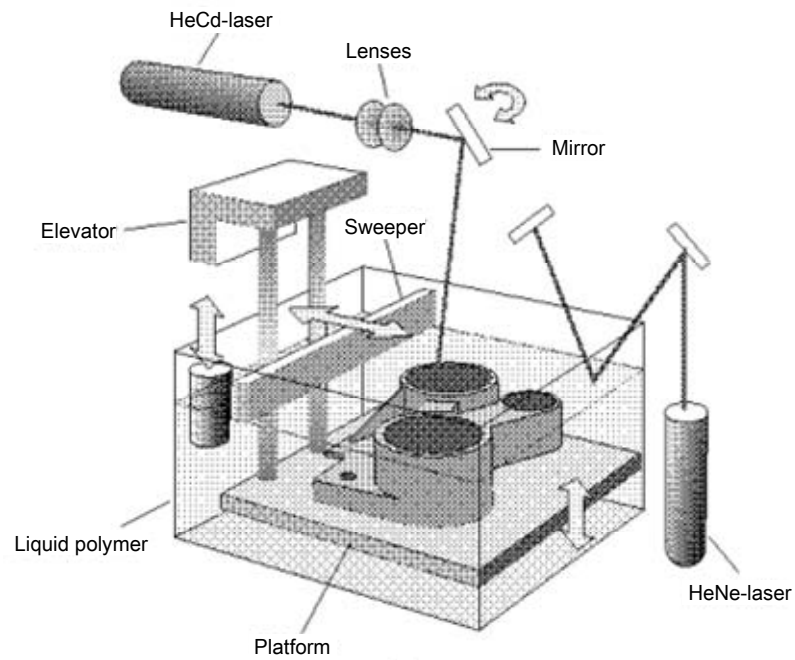


Figure 2.7: Schematic diagram of stereolithography[41].

CHAPTER THREE: HYBRID FLUIDIC INTERFACE

3.1 Design and assembly

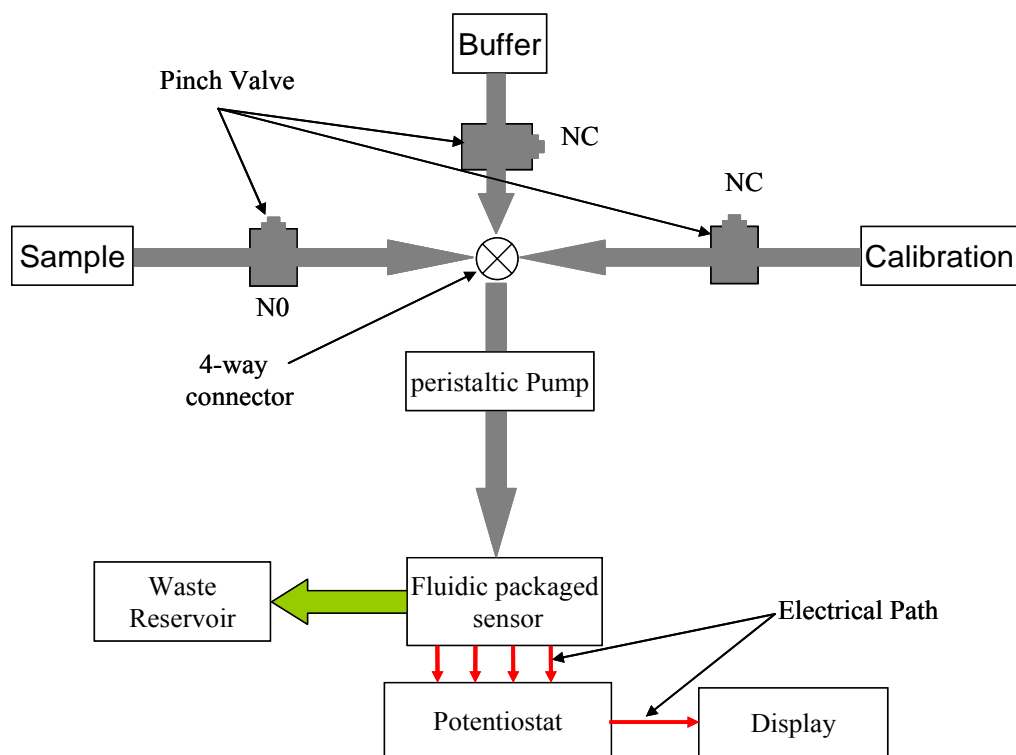


Figure 3.1: Block diagram of design scheme for a hybrid fluidic system.

For a flow-through type chemical sensor, initially small quantities of buffer solution need to be driven to the chemical sensor surface for cleaning, then the calibration solution for calibrating the sensor and finally the sample solution for testing. Figure 3.1 shows the design scheme used for building hybrid fluidic system for flow through type chemical sensor. The flows are driven by the pump from sample holder to waste reservoir, and the selection of the sample to be driven is made by actuating the valves. The sensor signal is measured using potentiostat for electrochemical type sensor.

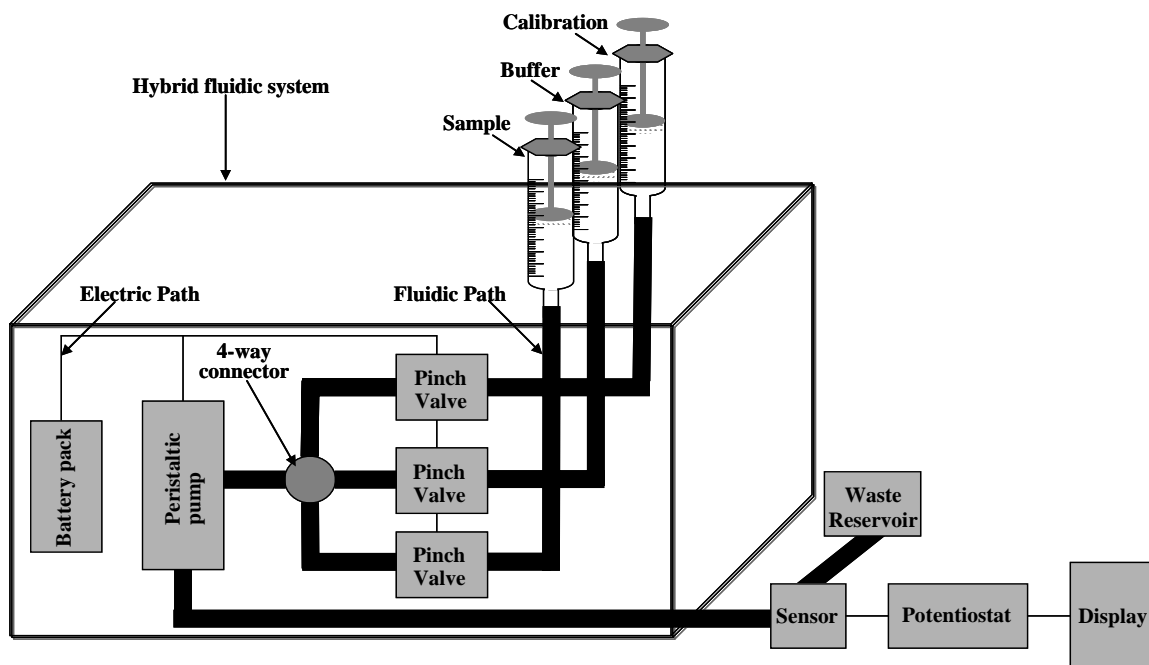


Figure 3.2: Schematic of hybrid fluidic system.

Figure 3.2 shows the schematic of a hybrid fluidic system. The fluidic system has three syringes to hold sample, buffer and calibration solution. A silicone tubing (1/32" dia) was used for the transport of the fluids. The fluids were driven by a peristaltic pump (Instechlabs, P625) with an intended flow rate range of 0.15-3.0 ml/min. A variable resistance potentiometer was used to control the flow rate.

Two types of pinch valves (normally open, normally closed) (Bio-Chem Valve Inc., 075P) were used to select the sample to be driven to the sensor chip. Figure 3.3 shows the actual view of a pump and a valve used in the hybrid fluidic system.

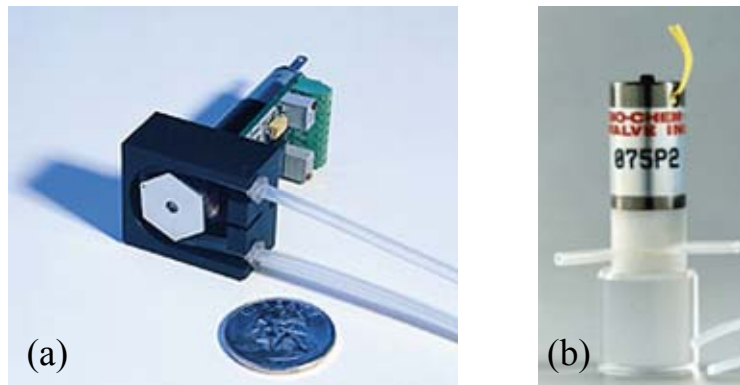


Figure 3.3: Actual view of (a) peristaltic pump and (b) pinch valve.

The pump and valves are powered by 12-volt battery pack. A normally-closed pinch valve was used for buffer and calibration selection, since these fluids are needed initially for little time to clean and calibrate the sensor. A normally-open valve was used for sample/analyte selection, since this fluid needs to be driven for long time. The adequate selection of the components helps reduce power consumption.

electrode in contact with the solution is necessary (and this electrode will have its own metal-solution potential difference) to measure the potential difference between the electrodes[38]. There is no potential gradient across the bulk of the solution phase under zero-current conditions. This means that an ion in the bulk solution phase will have no way of knowing whether electrodes exist, and will have no way of ascertaining its own potential relative to either of the electrodes. The region across where $\Delta\phi$ resides is broadly defined as the “electrical double layer,” and it is in the region of very high potential gradient (typically 10^6 V/cm) that all the chemical reactions takes place. The double layer has the electrical characteristics similar to that of a conventional capacitor [35].

The electrode where the chemistry of importance occurs is called the working electrode (W). The working electrode is at the ground as far as the outside world is concerned; it is positive relative to the bulk solution inner potential. The potential difference we wish to control is $\Delta\phi_w$ and the desired control point (DCP) needs to be indicated. The actual control point (ACP) as far as the circuit is concerned is at the reference electrode. The reference electrode is used as a potentiometric (always zero-current) probe to monitor $\Delta\phi_w$ relative to its own $\Delta\phi_r$. The counter is used to complete the circuit, allowing charge to flow through the cell. The DCP and ACP are closer together in the three electrode cell, they are still not the same. There will be iR drop error, albeit small. The total cell resistance has been divided into two parts: a compensated resistance R_c and an uncompensated resistance R_u [42].

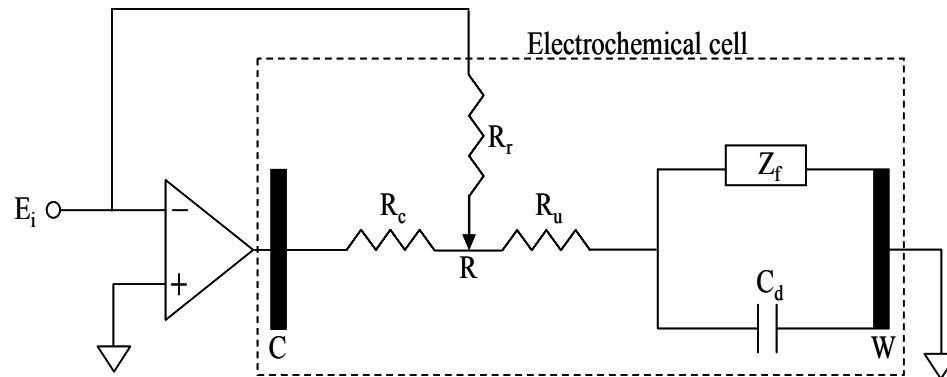


Figure 4.2: Equivalent circuit of a three electrode cell.

The equivalent circuit for the three electrode cell can be constructed using passive components as shown in figure 4.2. R_r is the reference electrode impedance, R_c is the compensated resistance, R_u is the uncompensated resistance, and the working electrode is connected to ground. The bulk-phase resistances are represented by R_c and R_u , the solution and electrode interphase components is represented by C_d (double-layer capacitance), and Z_f (faradaic impedance) has been added. When a faradaic reaction occurs, the working electrode interface takes on the character of a leaky capacitor [34]. Phenomenologically, one considers the charge stored in the double layer to leak away through some heterogeneous electron transfer reaction represented by the impedance, Z_f . In order to maintain the potential difference $\Delta\phi_w$ relative to reference electrode, additional charge must flow to replenish that being lost through Z_f . This is the function of the potentiostat and is realized using operational amplifiers.

4.2 Design and simulation

Figure 4.3 shows the block diagram of the potentiostat measuring system for three electrode chemical sensor.

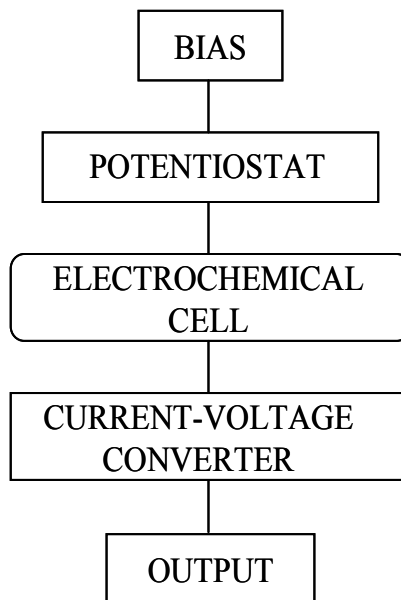


Figure 4.3: Block diagram of the measuring system for three electrode amperometric chemical sensor.

Potentiostat is a circuit for maintaining invariable the voltage between reference and working electrodes. The circuit compensates possible voltage losses due to the chemical solution. The I-V converter outputs a voltage proportional to the working electrode current and the output multimeter shows the current-voltage values to those corresponding to chemical concentration. An adjustable circuit to provide a constant cell polarization potential at the working electrode was designed using a zener diode.

The basic circuit of a potentiostat is represented by a feedback circuit, which compensates voltage drops generated between the working electrode and the reference probe. The circuit is shown in figure 4.4. The integrated circuit (IC) U1, operational amplifier, outputs a potential equal to potential for polarizing and initiate chemical reaction of importance at the working electrode plus losses originated in the solution.

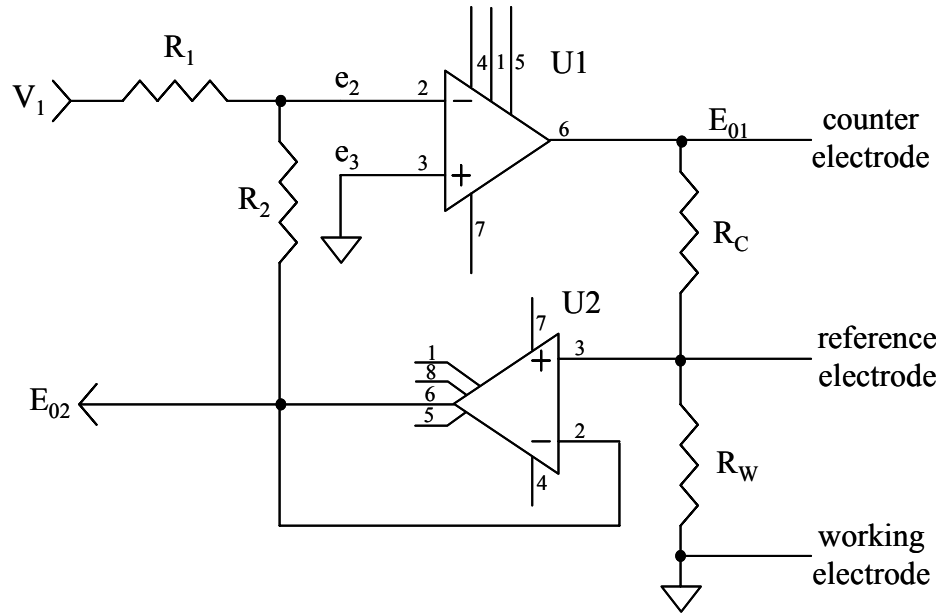


Figure 4.4: Schematic diagram of the potentiostat circuit.

The IC U2, is the sensor to feedback an error voltage through resistor R_2 . Consider the circuit shown in figure 4.4, R_c and R_w are the hypothetical resistors of charge-transfer resistance of the dissolution zones between counter and reference electrodes and between reference and working electrodes respectively.

For U1, with $e_3=0$, and $R_1=R_2$,

$$e_2 = \frac{1}{2}(v_1 - E_{02}) + E_{02}. \quad (1)$$

where V_1 is the polarizing input voltage to U1 and E_{02} is the output voltage signal from reference electrode.

The circuit U2, as voltage follower from the hypothetical network of R_c and R_w , works according to the equation shown below.

$$e_2 = \frac{R_w}{(R_w + R_c)}. \quad (2)$$

Combining (1) and (2) and making practical considerations like a very large open-loop amplification factor of the operational amplifier and the working and reference electrodes close together in the solution, the condition $R_w \lll R_c$ can be accepted. Then, we have the expression,

$$E_{02} = -V_1 \quad (3)$$

which means the reference electrode potential can be set ignoring R_w and R_c effects. This condition and the virtual ground in the I-V converter circuit, establish the potential difference between the reference and working electrodes, once preset, to be constant. The IC U1 is an operational amplifier of type TL081 with FET input, low noise, high slew rate and a high common mode rejection ratio (CMRR). The circuit U2, type CA3140, is a device with very high input impedance ($>10^{12}\Omega$), low noise, high CMRR. A potentiometer P8 was connected to provide offset adjustment.

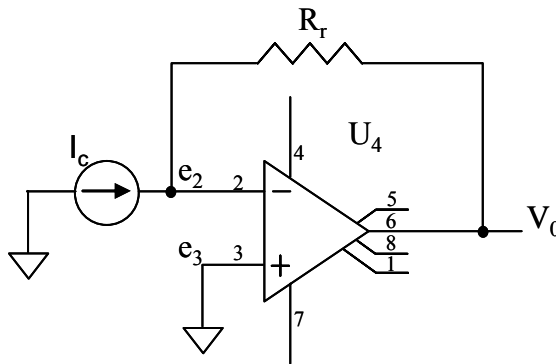


Figure 4.5: Circuit for current-voltage conversion.

The I-V configuration uses the condition of virtual ground on the input e_2 , which acts as a sum point. This is shown in figure 4.5 and can be expressed in the equation shown below.

$$I_c = -I_r \quad (4)$$

where I_c is the input current of this circuit. It also corresponds to the current passing by counter and working electrodes. The current I_r passes by the feedback resistor R_r . The output voltage V_0 of I-V converter is given by the equation below.

$$V_0 = -I_c R_r \quad (5)$$

Or

$$V_0 = I_r R_r \quad (6)$$

The output voltage of I-V converter will be proportional to current passing by the electrochemical cell from the counter to working electrodes.

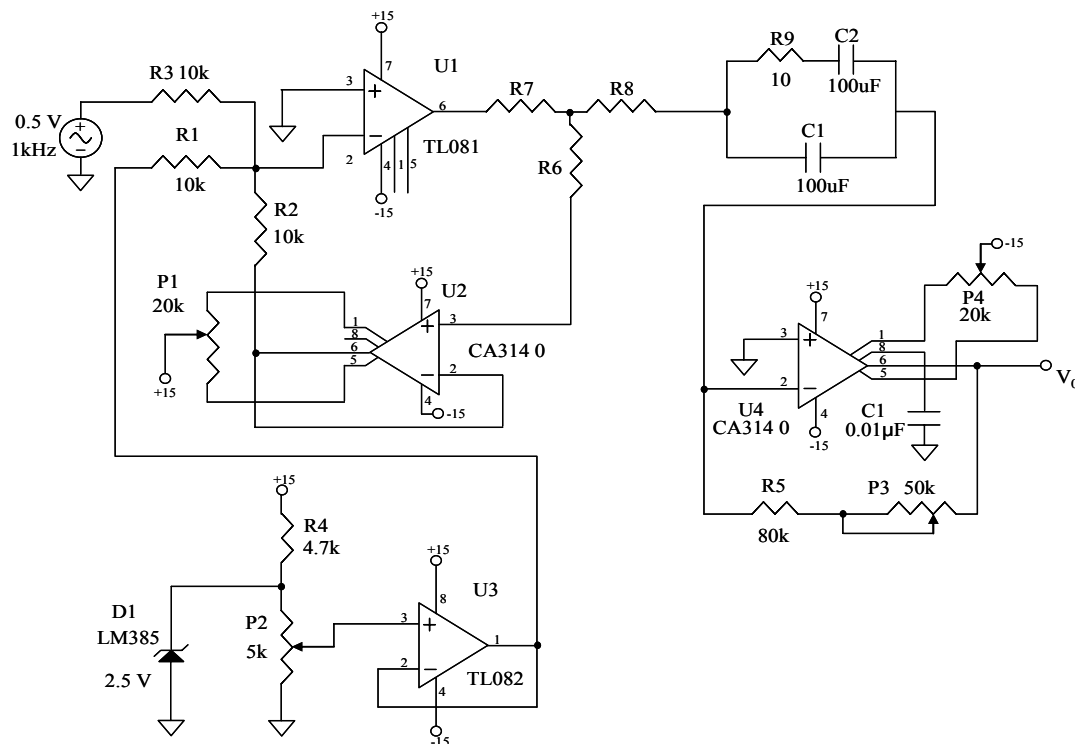


Figure 4.6: Circuit diagram of potentiostat for amperometric measurements in three electrode chemical sensor.

The complete circuit of potentiostat for amperometric measurement in three electrode chemical sensor is shown in figure 4.6. The IC U1 is the control amplifier responsible to keep the voltage between the reference and working electrodes constant to the preset voltage set through the IC U3. The control amplifier adjusts its output to automatically control the cell current so that the preset voltage difference is maintained between the working and reference electrodes. A small AC excitation signal is added to excess polarization at the working electrode. The bulk phase resistances values of R_c and R_u in equivalent circuit for electrochemical cell depend on solution conductivity, the distance between the two electrodes, and electrode geometry. In a cell with circular planes, the resistance between the counter electrode (radius r_a) and working electrode

(radius r_w) can be adequately estimated from the following equations from literature[38, 43].

$$R_s = \frac{1}{K\pi r_w (r_w + r_c)} \quad (7)$$

$$R_u = \frac{r}{K\pi r_w (r_w + r_w)} \quad (8)$$

In the above equations K ($\Omega\text{-cm}$)⁻¹ is the specific conductivity of the solution. The distance between working and reference electrode is represented by r . R_s is the total bulk phase resistance which is equal to R_c+R_u . The values of interfacial capacitance and faradaic impedance are assumed. The circuit was simulated using ModelSIM[®] circuit simulator (Mentor Graphics Corporation).

CHAPTER FIVE: RESULTS AND DISCUSSION

5.1 Interconnection

5.1.1 Microfluidic package

The microfluidic package was successfully fabricated using injection molding. Figure 5.1 shows a SEM picture of the interconnection hole formed with the microfluidic channel.

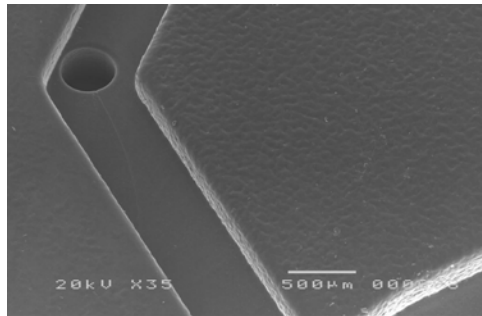


Figure 5.1: SEM picture of the interconnection hole in fluidic channel.

The standard inlet/outlet interconnection tubing of the microfluidic package made it possible to snap together multiple packages. Figure 5.2 shows the interconnected microfluidic packages.

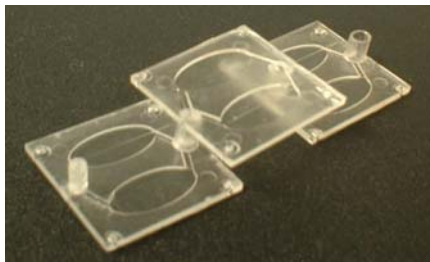


Figure 5.2: Interconnected fluidic packages.

A demonstration device with package used for testing is shown in figure 5.3.

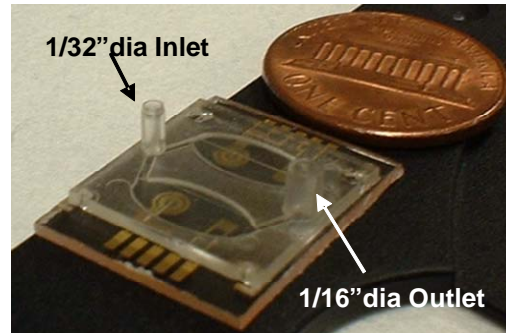


Figure 5.3: Assembled view of the microfluidic package with a chip based sensor.

5.1.2 Plug-in type package



Figure 5.4: Assembled view of the plug-in type package with micromachined sensor.

Figure 5.4 shows the fabricated package with sensor. Figure 5.4a and b shows the micromachined sensor placed in between the two pieces of the package. Commercially available electrical contact leads is fitted in the holes for measurement of signal from the sensor. Figure 2.9c shows the inserted plug-in type package with sensor into T-junction connector for online monitoring of the sample without the need for sample extract.

5.2 Hybrid fluidic system

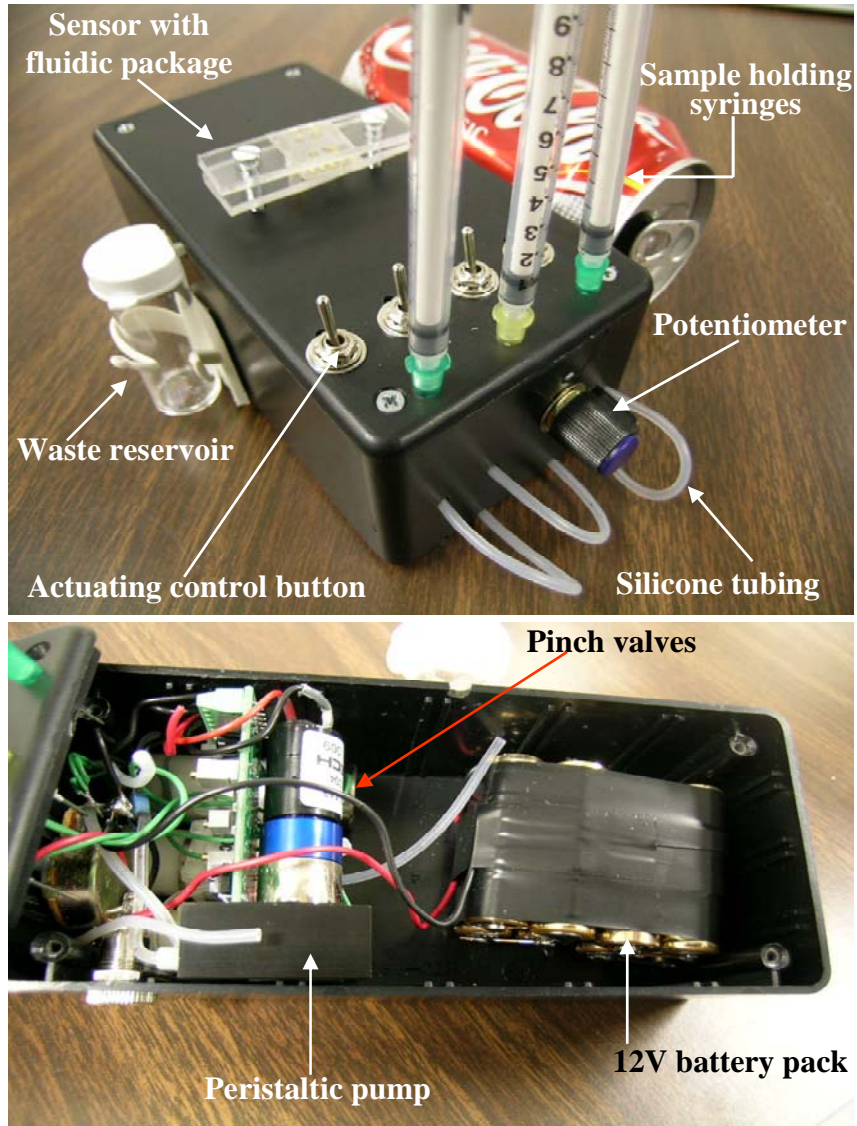


Figure 5.5: Hybrid fluidic system.

Figure 5.5 shows the completely assembled hybrid fluidic system using commercially available peristaltic pump and pinch valves. A silicone tubing is used for fluidic transport. Control buttons are used for actuating pump and valves. Syringes are

used for holding the samples. The flow rate can be controlled linearly by adjusting potentiometer. Figure 5.6 shows the change in flow rate with varying resistance.

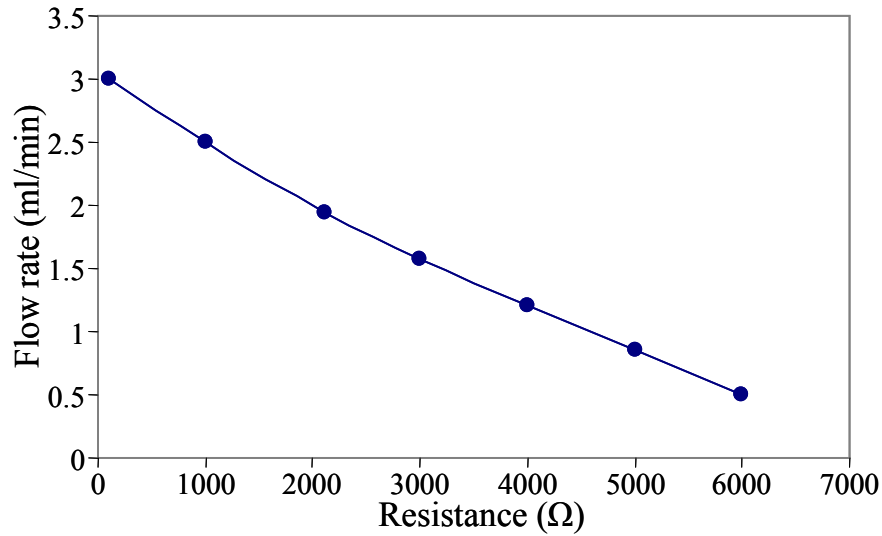


Figure 5.6: Flow rate as a function of resistance.

5.3 Potentiostat circuit simulation.

The potentiostat circuit was simulated for transient analysis to observe the output current and voltage for varying values of R_c and R_u in the equivalent electrochemical cell circuit. Figure 5.7 shows the block diagram of the potentiostat circuit. R_c and R_u values are dependent on structure, distance between the electrodes, and specific conductivity of the sample solution. The bulk phase resistances R_c , R_u were calculated by taking the values of specific conductivity of the KCl solution and distance between the electrodes from the above tested micromachined chlorine sensor using the equations (7), (8) mentioned in chapter 4.

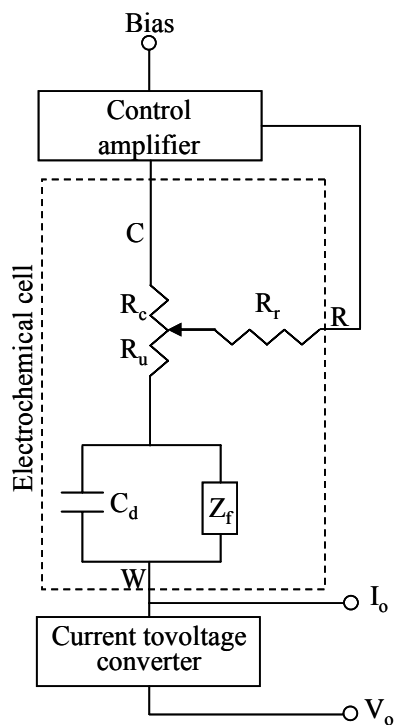


Figure 5.7: Block diagram of the potentiostatic circuit including equivalent circuit of an electrochemical cell.

Figure 5.8 shows the current output taken at the working electrode corresponding to 0.2M KCl specific conductivity solution equivalent values of R_c and R_u . The stable current outputs were tabulated and plotted as shown in figure 5.9. As observed in the graph, the variation in the current is very minute; this is because the faradaic impedance (Z_f) and double layer capacitance (C_{dl}) were kept constant for varying bulk phase resistance values. The voltage output at the C-V converter corresponding to current at the working electrode were tabulated and plotted as shown in figure 5.10.

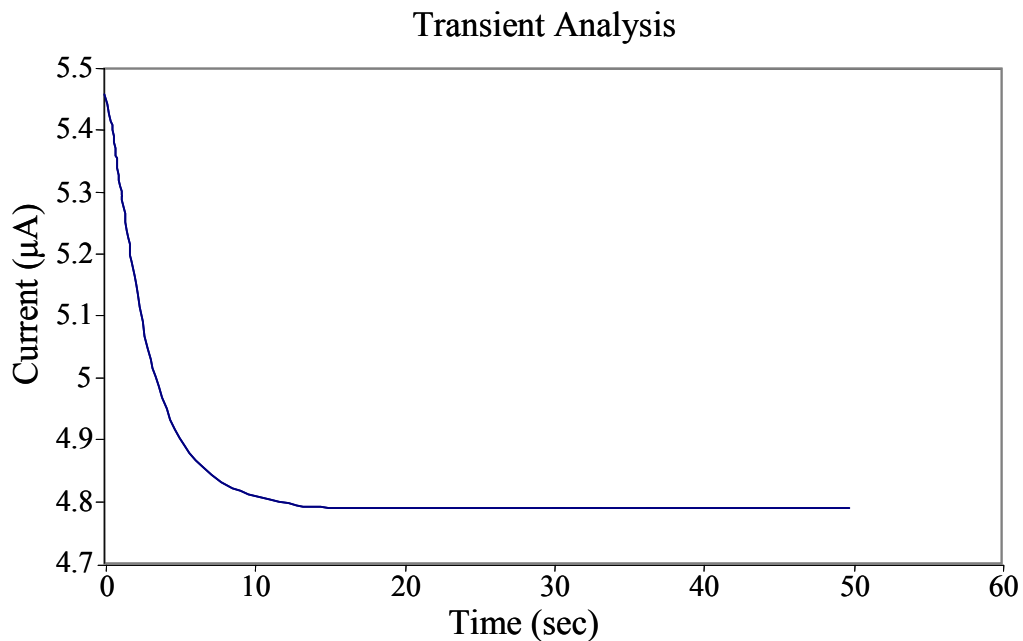


Figure 5.8: Time variation for current output at the working electrode.

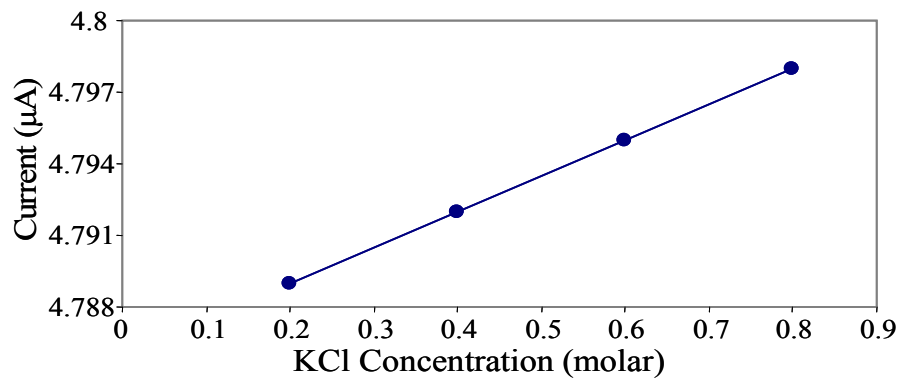


Figure 5.9: Current output for varying bulk resistance values corresponding to KCl concentration.

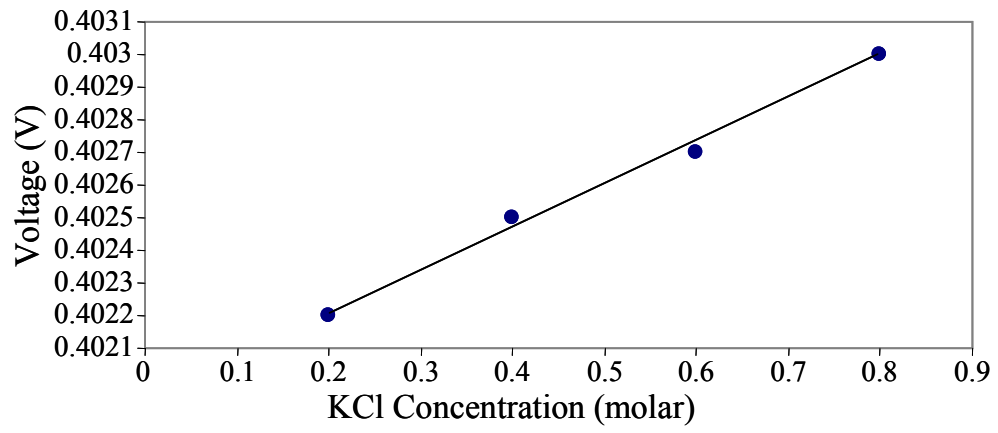


Figure 5.10: Voltage output for varying bulk resistance values corresponding to KCl concentration.

5.4 Instrumentation testing

5.4.1 Micromachined sensor

The sensors for testing were fabricated by metal deposition, photolithography, electroplating and etching. The dimensions are shown in figure 5.11. Figure 5.12 shows the fabricated sensors for testing.

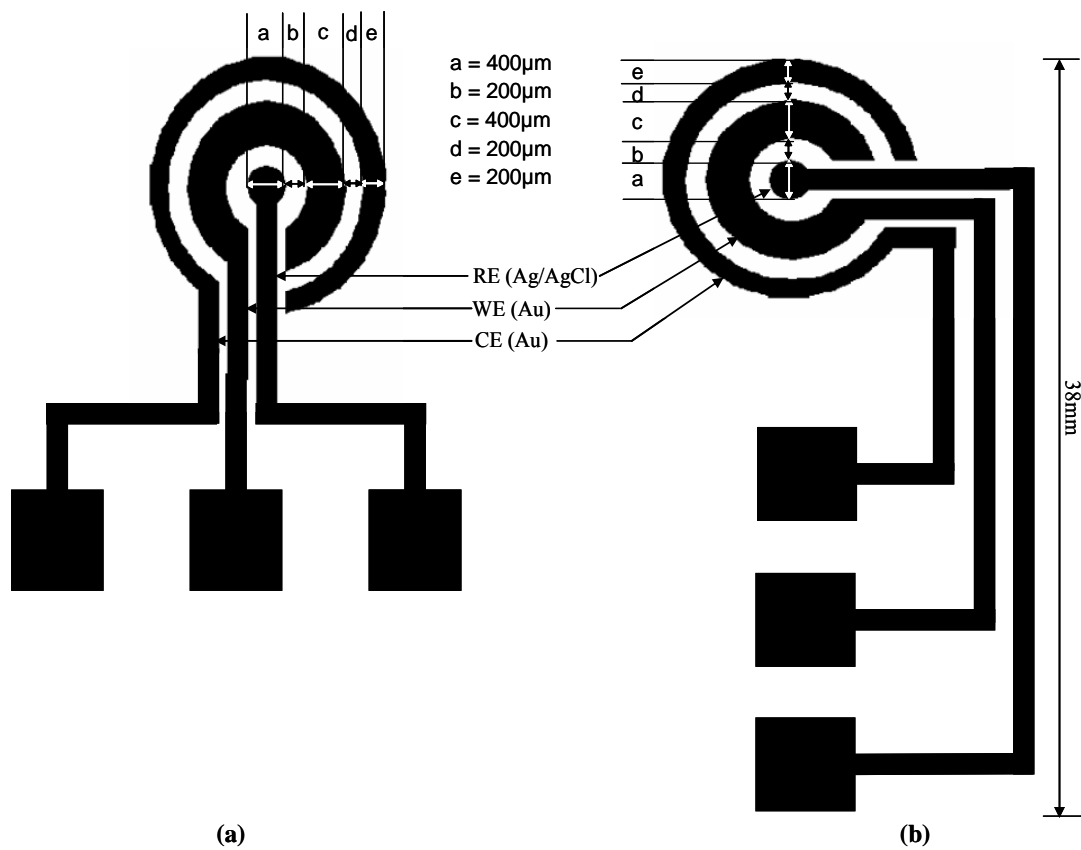


Figure 5.11: Dimensions of the three terminal amperometric chlorine sensor (a) flow-through type sensor, (b) plug-in type sensor.

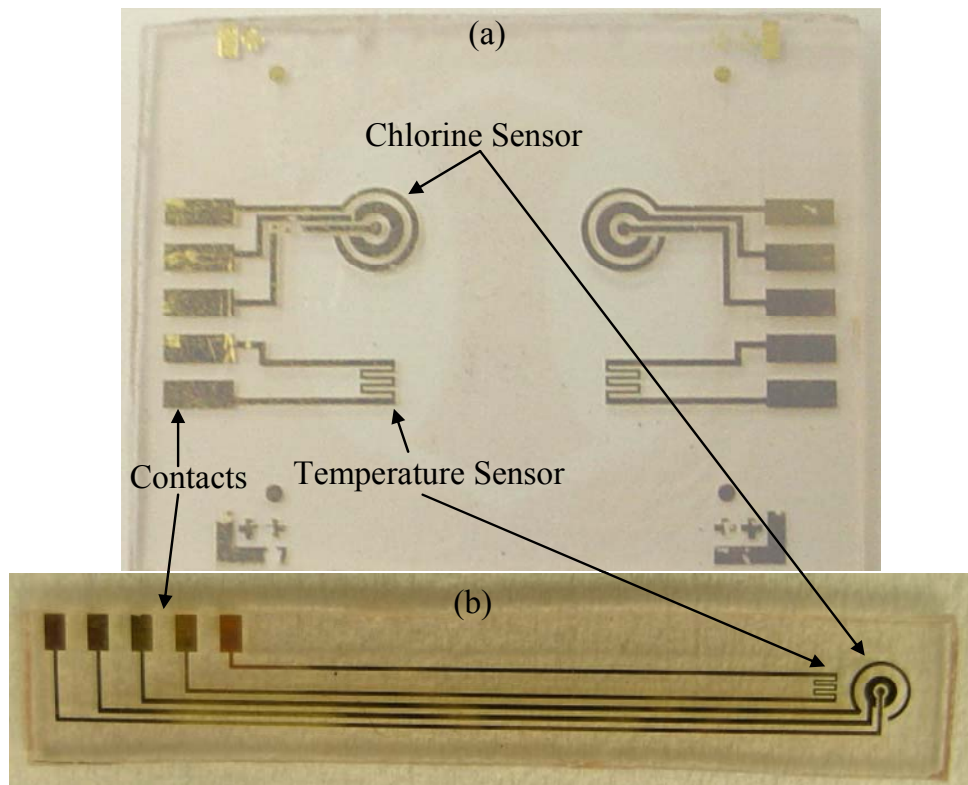


Figure 5.12: Fabricated sensors (a) flow-through type sensor, (b) plug-in type sensor.

5.4.2 Flow-through sensor instrument

Potentiostatic polarization experiments were performed on varying concentration of chlorinated DI water samples using Clorox[®]. Figure 5.13 shows the experimental setup for the flow through measurements using developed hybrid fluidic system and microfluidic package. In this case commercially available PalmSens potentiostat (Palm Instruments BV) and pocket pc (HP hx 2110) were used to measure and display the sensor output.

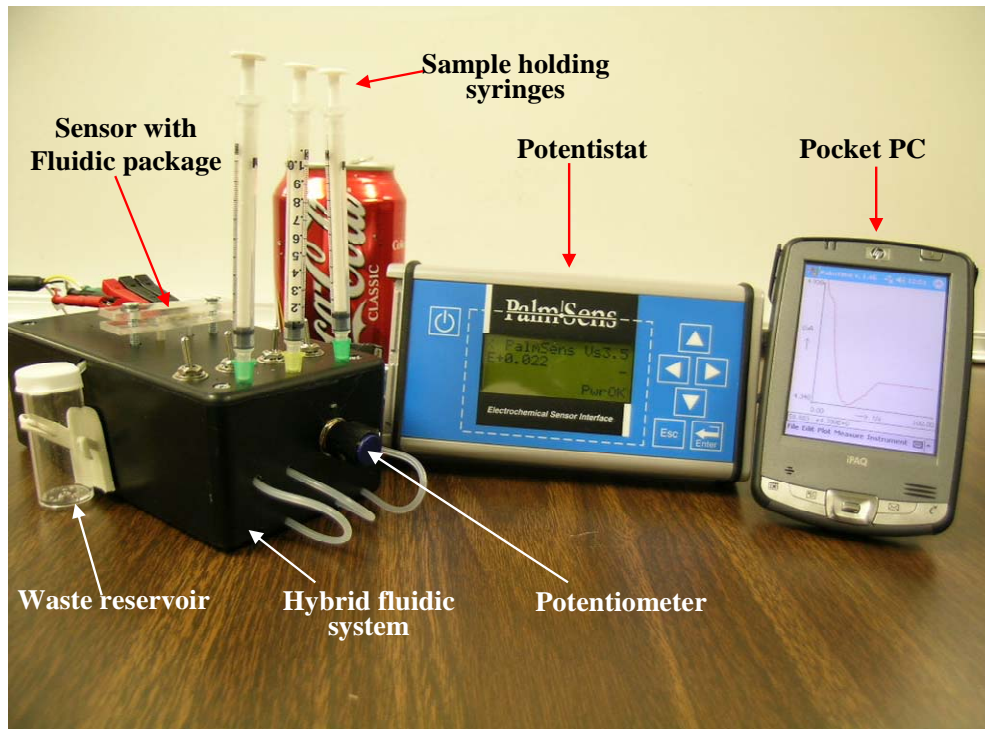


Figure 5.13: Experimental setup for flow through measurement.

The sample was introduced to the microfluidic packaged sensor from the sample holding syringes at a flow rate of 3ml/min. Figure 5.14 shows a potentiostatic polarization curve on sample with 1.6ppm chlorine concentration.

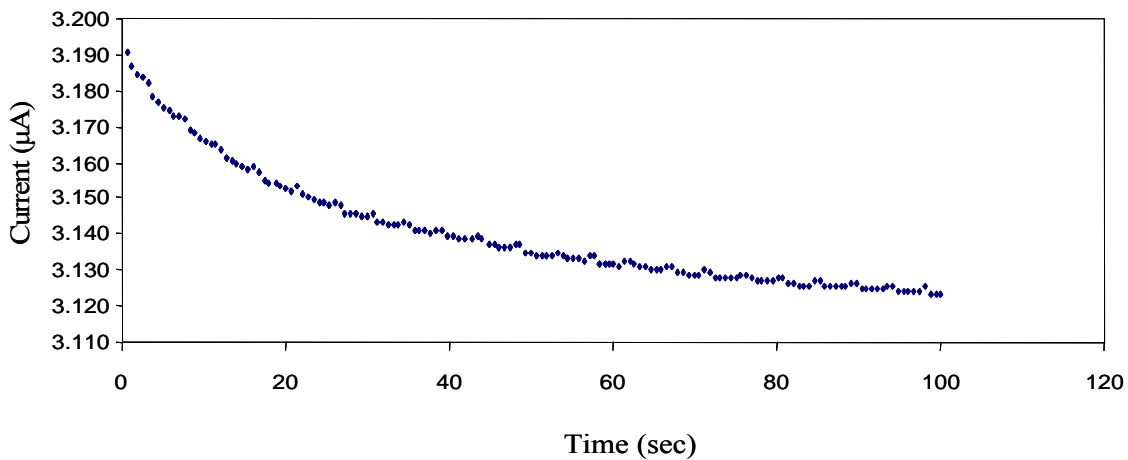


Figure 5.14: Time variation of sensor output measured in a solution with 1.6ppm chlorine under flow through conditions.

As can be observed from the graph the sensor took 100 seconds to attain a stable value. The stable current outputs from all the potentiostatic polarization experiment were plotted as shown in figure 5.15

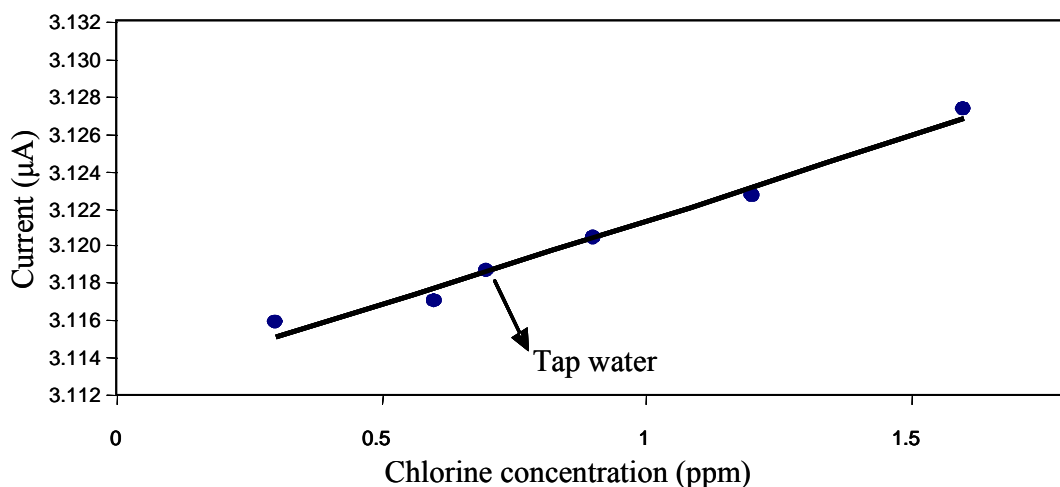


Figure 5.15: Sensor output current as a function of chlorine concentration.

5.4.3 Plug-in sensor instrument

Figure 5.16 shows the cyclic polarization curve for the standard solution of 0.1M KCl in DI water which was used to obtain the polarization potential of the sensor. The plug-in type packaged sensor is dipped in the sample under static condition. Electrochemical measurements were made from PalmSens potentiostat (Palm Instruments BV). The cyclic polarization was performed between -1V and 1V with respect to the reference electrode. From the results, the reduction potential of chlorine was obtained and used for performing amperometric measurements.

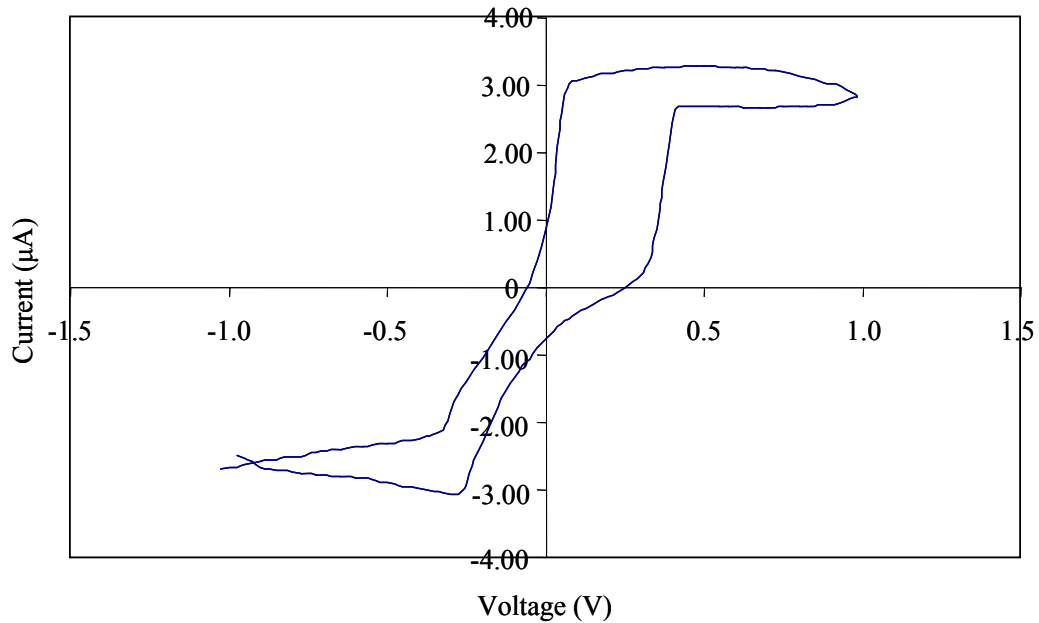


Figure 5.16: Cyclic polarization curve obtained from microfluidic packaged chlorine sensor using 0.1M KCl solution.

From the obtained reduction potential of chlorine by cyclic polarization curve, potentiostatic polarization experiments were performed with plug-in type packaged chlorine sensor. The experiments were conducted in static and dynamic conditions.

Static condition: In this experiment the plug-in type packaged sensor was dipped in the analyte which is under static condition. Standard solutions varying from 0.1M to 1M KCl in DI water was prepared to perform the potentiostatic polarization experiment. Figure 5.17 shows a potentiostatic polarization curve on sample with 0.1M KCl concentration.

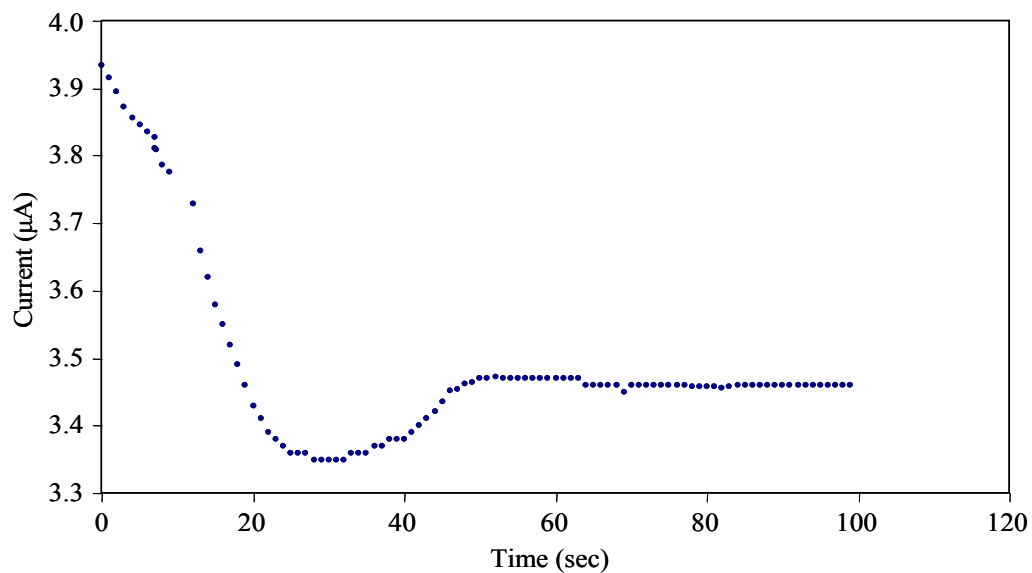


Figure 5.17: Time variation of sensor output measured in 0.1M KCl solution at static condition for chlorine concentration.

Potentiostatic polarization is performed for different samples. The stable current output from all the experiment under static condition was plotted as shown in figure 5.18.

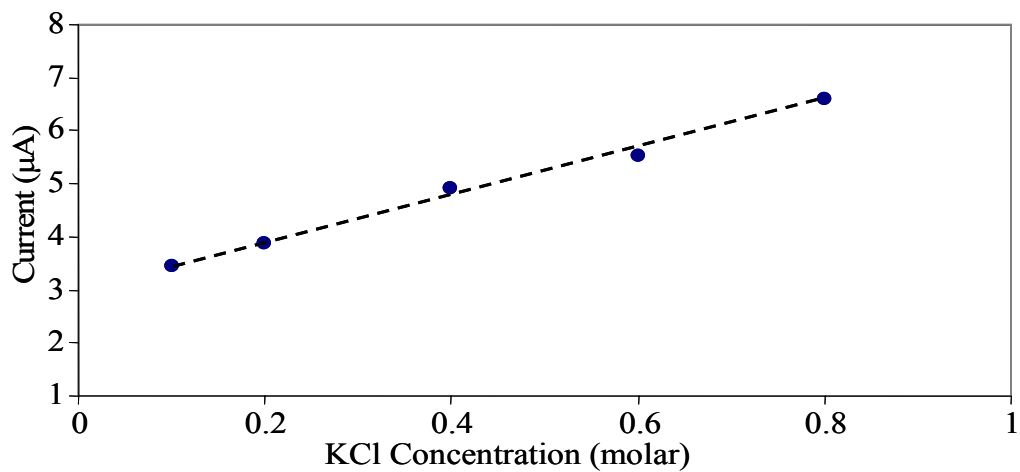


Figure 5.18: Sensor output current as a function of KCl concentration.

Dynamic condition: In this case the plug-in type packaged sensor was inserted in the T-connector in the sample flow stream. Figure 5.19 shows the experimental setup for dynamic measurements in the flow stream without sample extraction.

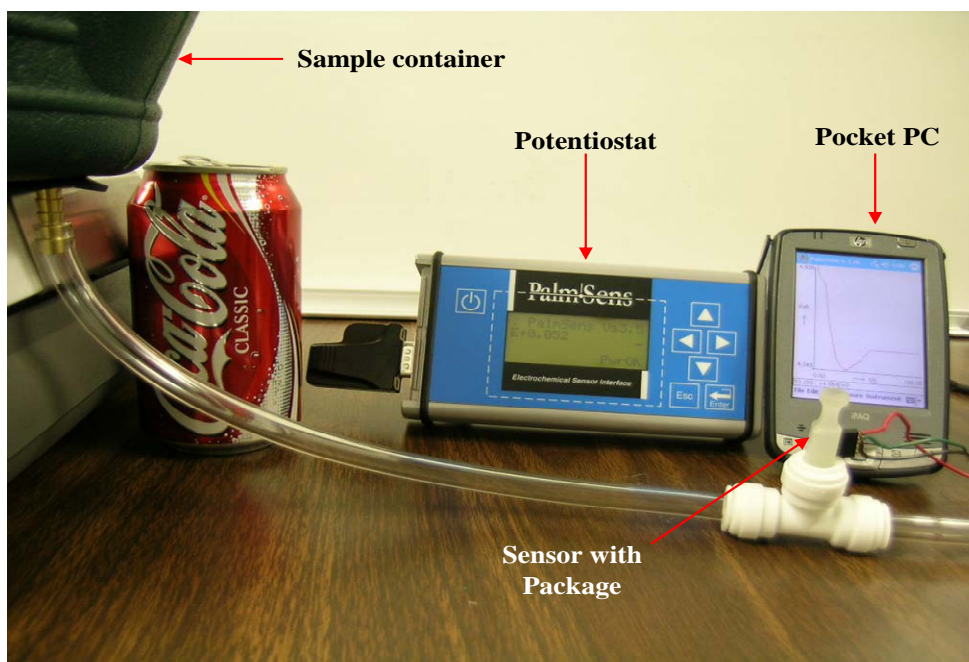


Figure 5.19: Experimental setup for dynamic condition measurement using plug-in type packaged chlorine sensor.

Figure 5.20 shows the potentiostatic polarization on sample with 0.4M KCl concentration under dynamic condition at flow rate of 15ml/min. a fairly stable output was observed under the flow rate of 15ml/min. A stability period of 100 second was needed for sensor signal to attain fairly constant value of the current. The constant value of the current was matching with the static condition, which validates the use of plug-in type sensor for online monitoring.

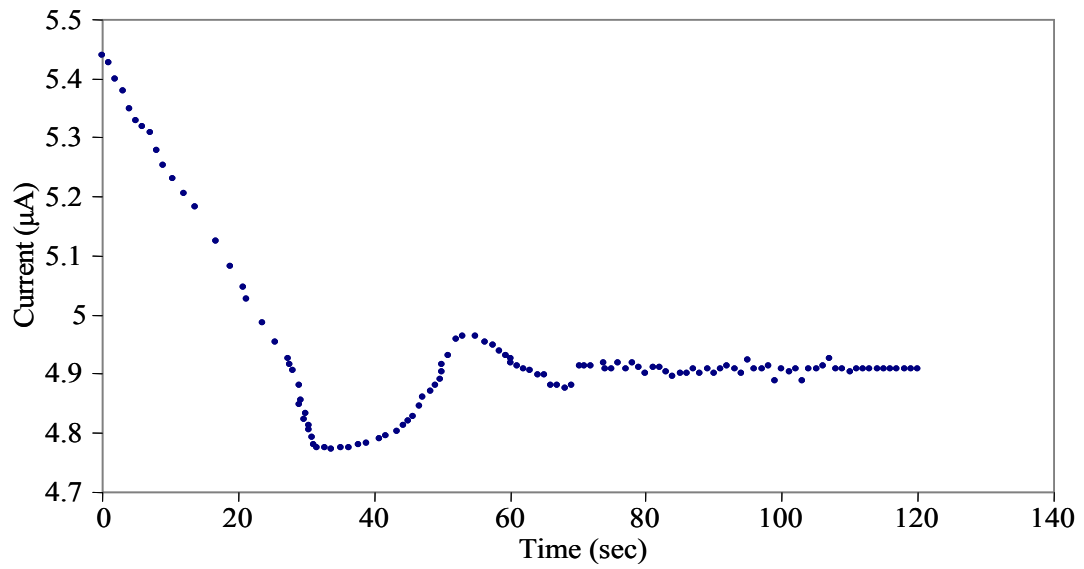


Figure 5.20: Time variation of sensor output measured in 0.4M KCl solution at dynamic condition for chlorine concentration.

CHAPTER SIX: CONCLUSION AND FUTURE WORK

6.1 Conclusion

In this work, interconnection methods of micromachined chip devices, a hybrid fluidic interface system, and measurement circuitry for completing instrumentation were studied. The interconnection method is based on one body construction which includes fluidic channels and chambers with standard interconnection tubings. In addition, a plug-in type interconnection method for a large amount of flow samples was studied. The hybrid fluidic system was developed using a commercially available peristaltic pump and pinch valves. Micromachined electrochemical sensors were tested with the developed methods and hybrid fluidic system for flow-through measurement. The results obtained from testing validate the use of the developed interconnection methods and interface for a portable instrument. The potentiostat circuit for amperometric measurement was investigated. The circuit was designed and simulated in ModelSIM circuit simulator. Transient analysis of the circuit was done in the simulation for varying values of bulk phase resistances. The simulated output showed linear current and voltage values, which would be useful to realize an integrated potentiostat for miniaturization of the chemical analysis instrument.

6.2 Future work

The potentiostat simulation results need to be implemented into a real circuit for a truly instrument. An automated flow regulation as well as incorporation of a display will be investigated.

REFERENCES

- [1] H. T. G. v. Lintel, F. C. M. v. D. Pol, and S. Bouwstra, "A piezoelectric micropump based on micromachining of silicon," *Sensors and Actuators*, vol. 15, pp. 153-157, 1988.
- [2] S. Shoji, S. Nakagawa, and M. Esashi, "Micropump and sample-injector for integrated chemical analyzing systems," *Sensors and Actuators A: Physical*, vol. 21, pp. 189-192, 1990.
- [3] A. Manz, F. Bessoth, Y. Xu, and P. Monaghan, "Miniaturizing conventional analytical methods: Micro reactors for bioassays and cell growth," *Conference proceedings of Biosensors 2002*, pp. 915-918, 2002.
- [4] M. J. Madou, *Fundamentals of Microfabrication*, 2nd edition ed. Boca Raton: CRC Press LLC, 1997.
- [5] M. J. Madou and J. Florkey, "From batch to continuous Manufacturing of Microbiomedical Devices," *American Chemical Society*, vol. 100, pp. 2679-2692, 2000.
- [6] C. R. Tamanaha, L. J. Whitman, and R. J. Colton, "Hybrid macro–micro fluidics system for a chip-based biosensor," *Journal of Micromechanics and Microengineering*, vol. 12, pp. N7-N17, 2002.
- [7] P. Gravesen, J. Branebjerg, and O. S. Jensen, "Microfluidics-a review," *Journal of Micromechanics and Microengineering*, vol. 3, pp. 168-182, 1993.

- [8] H. Mizoguchi, M. Ando, T. Mizuno, T. Takagi, and N. Nakajima, "Design and fabrication of light driven micropump," *Conference proceedings of IEEE Micro Electro Mechanical Systems*, pp. 31-36, 1992.
- [9] B. Bustgens, W. Bacher, W. Menz, and W. K. Schomburg, "Micropump manufactured by thermoplastic molding," *Conference proceedings of IEEE Micro Electro Mechanical Systems*, pp. 18-21, 1994.
- [10] S. Böhm, W. Olthuis, and P. Bergveld, "A plastic micropump constructed with conventional techniques and materials," *Sensors and Actuators*, vol. 77, pp. 223-228, 1999.
- [11] R. Zengerle and H. Sandmaier, "Microfluidics," *Conference proceedings of IEEE Symposium on Micro Machine and Human Science*, pp. 13-20, 1996.
- [12] D. Jaeggi, B. L. Gray, N. J. Mourlas, B. P. v. Driehuisen, K. R. Williams, N. I. Maluf, and G. T. A. Kovacs, "Novel interconnection technologies for integrated microfluidic systems," *Conference proceedings of Solid-state Sensor and Actuator Workshop*, pp. 112-115, 1998.
- [13] E. Meng, S. Wu, and Y.-C. Tai, "Silicon couplers for microfluidic applications," *Journal of Analytical Chemistry*, vol. 371, pp. 270-275, 2001.
- [14] T.-J. Yao, S. Lee, W. Fang, and Y.-C. Tai, "Micromachined Rubber O-ring Micro-Fluidic Couplers," *Conference proceedings of IEEE Micro Electro Mechanical Systems*, pp. 624-627, 2000.

- [15] A. Puntambekar and C. H. Ahn, "Self-aligning microfluidic interconnects for glass- and plastic-based microfluidic systems," *Journal of Micromechanics and Microengineering*, vol. 12, pp. 35-40, 2001.
- [16] A. V. Pattekar and M. V. Kothare, "Novel microfluidic interconnectors for high temperature and pressure applications," *Journal of Micromechanics and Microengineering*, vol. 13, pp. 337-345, 2003.
- [17] J.-H. Tsai and L. Lin, "Micro-to-macro fluidic interconnectors with an integrated polymer sealant," *Journal of Micromechanics and Microengineering*, vol. 11, pp. 577-581, 2001.
- [18] C. Grosjean and Y.-C. Tai, "A Thermopneumatic Peristaltic Micropump," *Conference proceedings of IEEE Transducers*, pp. 1776-1779, 1999.
- [19] D. J. Laser, A. M. Myers, S. Yao, K. F. Bell, K. E. Goodson, J. G. Santiago, and T. W. Kenny, "Silicon Electroosmotic Micropumps for Integrated Circuit Thermal Management," presented at IEEE Transducers, Boston, MA, USA, 2003.
- [20] E. Kai, T. Pan, and B. Ziaie, "A robust low-cost PDMS peristaltic micropump with magnetic drive," *Conference proceedings of Solid-State Sensor, Actuator and Microsystems Workshop*, pp. 270-273, 2004.
- [21] X. Yang, C. Grosjean, Y.-C. Tai, and C.-M. Ho, "A MEMS Thermopneumatic Silicone Membrane Valve," *Conference proceedings of IEEE Micro Electro Mechanical Systems*, pp. 114-118, 1997.

- [22] C. Grosjean, X. Yang, and Y.-C. Tai, "A practical thermopneumatic valve," *Conference proceedings of IEEE Micro Electro Mechanical Systems*, pp. 147-152, 1999.
- [23] J. Fahrenberg, D. Mass, W. Menz, and W. K. Schomburg, "Active microvalve system manufactured by the LIGA process," *Conference proceedings of Actuator*, pp. 71-74, 1994.
- [24] J. Fahrenberg, W. Bier, D. Maas, W. Menz, R. Ruprecht, and W. K. Schomburg, "A microvalve system fabricated by thermoplastic moulding," *Journal of Micromechanics and Microengineering*, vol. 5, pp. 169-171, 1995.
- [25] H. Jerman, "Electrically-activated, normally-closed diaphragm valves," *Conference proceedings of IEEE Transducers*, pp. 1045-1048, 1991.
- [26] M. Zbedlick, R. Anderson, J. Jankowski, B. Kline-Schoder, L. Christel, R. Miles, and W. Weber, "Thermopneumatically Actuated Microvalves and Integrated Electro-Fluidic Circuits," *Conference proceedings of Solid-State Sensor and Actuator Workshop*, pp. 251-255, 1994.
- [27] W. H. Grover, A. M. Skelley, C. N. Liu, E. T. Lagally, and R. A. Mathies, "Practical valves and pumps for large-scale integration into microfluidic analysis devices," *Conference proceedings of Micro Total Analysis System (μ -TAS)*, pp. 136-138, 2002.
- [28] O. Geschke, H. Klank, and P. Telleman, *Microsystem Engineering of Lab-on-a-Chip Devices*. Denmark: WILEY-VCH, 2004.

- [29] S. Shoji and M. Esashi, "Microflow devices and systems," *journal of Micromechanics and Microengineering*, vol. 4, pp. 157-171, 1994.
- [30] A. Olsson, P. Enoksson, G. Stemme, and E. Stemme, "Micromachined flat-walled valveless diffuser pumps," *J. Microelectromechanical Systems*, vol. 6, pp. 161-166, 1997.
- [31] M. Stehr, S. Messner, H. Sandmaier, and R. Zengerle, "A new micropump with bidirectional fluid transport and selfblocking effect," *Conference proceedings of IEEE Micro Electro Mechanical Systems*, pp. 485-490, 1996.
- [32] P. Woias, "Micropumps—past, progress and future prospects," *Sensors and Actuators B: Chemical*, vol. 105, pp. 28-38, 2005.
- [33] J. Janata, *Principles of Chemical sensors*: Plenum Press, New York, 1990.
- [34] A. J. Bard and L. R. Faulkner, *Electrochemical Methods Fundamentals and Applications*, 2nd ed. Newyork: John Wiley & Sons, 2001.
- [35] Alphasense-Limited, "Designing a potentiostatic circuit," <http://www.alphasense.com/Product%20page/Products/Application%20Notes/Toxic/AAN%20105.PDF>, 2003 February.
- [36] Biologic-Science-Instruments, "Potentiostat stability mystery explained," <http://www.bio-logic.info/potentiostat/notes/Potentiostat%20stability.pdf>.
- [37] Research-Solutions-&-Resoures, "Potentiostat Architectures - Active I/E Converters," <http://www.consultrsr.com/resources/pstats/design.htm>.
- [38] P. T. Kissinger and W. R. Heineman, *Laboratory Techniques in Electroanalytical Chemistry*: Marcel Dekker INC, New york, 1996.

- [39] P. R. Hernandez, C. A. Galan, A. Morales, and S. Alegret, "Measuring System for Amperometric Chemical Sensors using The Three-Electrode Technique for Field Application," *Journal of Applied Research and Technology*, pp. 107-113, 2002.
- [40] D. C. Duffy, J. C. McDonald, O. J. A. Schueller, and G. M. Whitesides, "Rapid Prototyping of Microfluidic Systems in Poly(dimethylsiloxine)," *Journal of Analytical Chemistry*, vol. 70, pp. 4974-4984, 1998.
- [41] Stereolithography.com, "Rapid Prototyping Techniques," <http://stereolithography.com/rapidprototyping.php>.
- [42] V. I. Ogurtsov, A. Mathewson, and M. M. Sheehan, "Analysis of specification of an electrode type sensor equivalent circuit on the base of impedance spectroscopy simulation," *Journal of physics*, vol. 10, pp. 325-328, 2005.
- [43] J. E. Mumby and S. P. Perone, "Potentiostat and Cell Design for the study of Rapid electrochemical Systems," *Journal of Chemical Instrumentation*, vol. 3, pp. 1187-1196, 1983.